Chapter 9
Novel Imaging for Treatment Planning or Tumor Response

Adam Gladwish and Kathy Han

Abstract Anatomic imaging has long represented an integral part of modern radiotherapy, from planning, image-guidance to response evaluation. Functional imaging modalities now allow oncologists to supplement these anatomic images with functional maps, to elucidate the underlying biologic processes of cancer and allow delineation of both physical and biologic target volumes. Prescription of dose to this combination, commonly referred to as dose painting, represents an attractive avenue to further improve the therapeutic ratio of radiotherapy. This chapter focuses on the integration of novel imaging techniques and their role in delineating biologic radiotherapeutic targets, organized by well-known principles in radiobiology: tumor repopulation, reoxygenation, and repair. Focus is largely on clinically available imaging modalities, including positron emission tomography (PET) with various targeted radionuclides and functional magnetic resonance imaging (MRI). Other potential preclinical techniques are highlighted where relevant, particularly as they apply to promising translational concepts. Emphasis is placed on integration into treatment planning, adaptive treatment modification, and posttreatment response assessment.

Keywords Functional imaging • Image-guided radiotherapy • Dose painting • Biologic targeting • Novel imaging • MRI • PET • Magnetic resonance spectroscopy • FDG • Hypoxia imaging

Introduction

Radiotherapy is primarily a locoregional treatment modality, capable of delivering tumoricidal doses to both areas of gross disease and those at high risk of harboring microscopic spread. Therefore, by definition radiotherapy relies on the ability to

A. Gladwish • K. Han (✉)
Princess Margaret Cancer Centre, Department of Radiation Oncology, University of Toronto, 610 University Ave., Toronto, ON, Canada M5G 2M9
e-mail: adam.gladwish@sunnybrook.ca; kathy.han@rmp.uhn.on.ca

P.J. Tofilon, K. Camphausen (eds.), *Increasing the Therapeutic Ratio of Radiotherapy*, Cancer Drug Discovery and Development,
DOI 10.1007/978-3-319-40854-5_9

accurately focus treatments to these regions, while simultaneously avoiding healthy normal tissue as much as possible. This forms the foundation of the therapeutic ratio in radiation-based treatments. Imaging is intrinsic within this process and as imaging technology has evolved, so too has modern radiotherapeutic techniques. Standard two-dimensional simulator-based planning has given way to three- and four-dimensional volume-based planning, based on improved anatomical and temporal delineation with both computed tomography (CT) and magnetic resonance imaging (MRI). Target definitions have evolved in parallel to advancing imaging techniques, and the latest International Commission on Radiation Units (ICRU) now outlines a host of anatomic-, clinical-, and geometric-based subvolumes which ultimately add together to produce the planning target volume (PTV). Furthermore, where these volumes were previously exclusively treated with homogenous doses based on predefined field borders, the aforementioned increases in imaging capability along with larger computational reserve have led to increasing use of intensity-modulated radiation therapy (IMRT) and volumetric modulated arc therapy (VMAT), whereby radiation doses can be sculpted around target volumes, further sparing the surrounding organs at risk (OARs). This increase in conformity has allowed for tumor doses to be escalated while maintaining consistent OAR doses, leading to further widening of the therapeutic window [1].

The rise of functional imaging offers promise of yet another target and perhaps a new paradigm for radiation oncologists, namely, the prescription of dose based on the intrinsic biology of the tumor being treated. This has been previously described as "dose painting" and has the theoretical advantage of being able to differentially target radiosensitive and radioresistant areas of disease, thereby maximizing the use of dose escalation to the regions that truly benefit. The concept of radiation sensitivity is most often discussed in terms of the classic tenants of radiobiology, the "4 Rs": the differential *r*epair of tumor and normal cells, the *r*edistribution of cells into more or less radiosensitive phases of the cell cycle, and the *r*epopulation and *r*eoxygenation of tumor cells between fractions (a fifth "*R*"—intrinsic radiosensitivity was introduced later to account for empirical data not explained by the other four). Advances in functional imaging provide the opportunity to directly measure and map these properties, offering a potential framework for modulated dose delivery. This chapter will review the current standard workflow of radiotherapy from treatment planning to tumor response assessment. This will provide a backbone on which to discuss various novel imaging modalities and their role in identifying and defining radiotherapeutic targets as well as characterizing post-treatment response.

Modern Radiation Therapy and Response Assessment

After the decision is made to proceed with radiotherapy, the standard workflow of modern radiotherapy typically dictates a process of treatment simulation, target/OAR delineation, radiation planning, quality assurance check, daily treatment verification, and post-treatment response assessment based on clinical exam, diagnostic imaging, and pathology where relevant (Fig. 9.1). Currently, X-ray-based imaging (helical CT, cone-beam CT scan, kV orthogonal, and MV portal imaging) represents the backbone

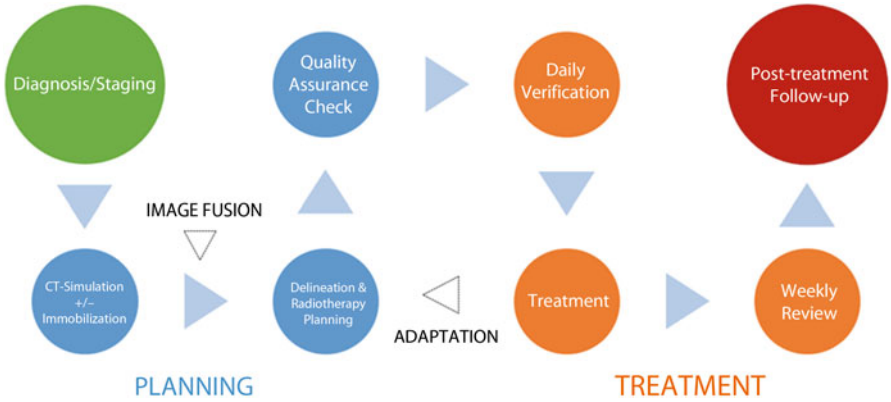

Fig. 9.1 Schematic representation of present radiotherapy workflow pathway

of this workflow. Initial simulation scans are acquired in the "treatment position," i.e., patients are scanned as they will be treated on a daily basis. These imaging datasets are then transferred to a planning system where the targets and OARs are delineated. Any adjunct information via clinical exam or other imaging modalities must be adapted to the current simulation images, sometimes objectively with image fusion and other times subjectively based on the clinical interpretation. Target volumes are defined according to the ICRU definitions, and a radiotherapy plan and dosimetric map are created based on these target volumes and pertinent OARs [2]. The plan then undergoes a quality assurance check and patients begin daily treatment. Once on treatment, the patient is set up based on the initial CT-simulation parameters and verified via some form of imaging, from 2D portal images to 3D/4D cone-beam CT scans (CBCT). After completion of treatment, the patient is seen in follow-up and evaluated with clinical exam ± imaging to determine the disease response.

To date the most impactful strategy to improve the therapeutic ratio in radiotherapy has involved improvements in the accuracy and precision of radiation delivery. This has been accomplished through improved anatomic planning images (e.g., higher-resolution CT, MRI simulators) to better delineate gross disease, advancing knowledge of patterns of relapse to better define the clinical target volume (CTV) and improved immobilization and daily image-guided imaging technologies to reduce uncertainties surrounding radiation delivery. The introduction of novel imaging modalities offers an opportunity to synergistically complement these with the ability to image and target differential tumor biology.

Dose Painting

The idea of targeting tumor subvolumes based on functional imaging is often referred to as "dose painting", a term coined by Ling and colleagues in 2005 [3]. The concept is to incorporate the quantitative output of a functional imaging

modality directly into the dose prescription. This can be done as coarsely as to prescribe two tumor prescriptions, i.e., the anatomic GTV and the biologic GTV, or as finely as a prescription for each voxel scaled on the biologic parameter in question. The latter approach was first proposed by Bentzen and was coined "dose painting by numbers", referencing the popular children's coloring technique [4]. Needless to say, there are innumerable intermediaries between these two ends of the spectrum.

The concept of dose painting is integral to the process of exploiting personalized tumor biology with radiotherapy, either by local escalation or de-escalation to resistant or sensitive tissues, respectively. The realization of this technique requires a rigorous preliminary evaluation, including assessing each modality's ability to quantify a relevant oncologic parameters, how said parameters are affected by treatment, and ultimately determining a clinically relevant dose–response relationship. Furthermore, the feasibility of integration of these new modalities will require careful quality assurance testing regarding the interaction with the current radiotherapy workflow.

Functional Imaging and the Basic Radiobiology

The radiobiologic principles—4 Rs—were first described by Withers as a means of explaining the tumoricidal effects of radiotherapy [5]. Withers described the differential repair, cell cycle redistribution, repopulation of tumor cells, and reoxygenation. These concepts fit well with the empirical evidence of differential cell kill noted in standard fractionated radiotherapy and observed oxygen enhancement. Intrinsic radiosensitivity was added to this framework over a decade later by Steel et al. as a means of rationalizing the differential cell kill effects based on tumor histology [6]. Over the past 30–40 years since these concepts were introduced, the understanding of cancer biology has grown exponentially, punctuated with the translational success of molecularly targeted agents in clinical care. Nonetheless, the original 4 Rs remain a fundamental pillar of radiotherapy due to their ability to explain empiric observations, with literature consistently being published to better explain the molecular underpinnings of this success [7]. As such, the 4 Rs provide a natural and useful framework in which to discuss the integration of functional imaging within the context of radiotherapy and the potential for optimizing the therapeutic ratio (Fig. 9.2). The workflow outlined in Fig. 9.1 also illustrates the potential for integration of adjunct imaging with adaptation. The following sections will describe the role of functional imaging modalities within this framework and highlight both current clinical applications and potential for future integration of ongoing translational research. We limit the discussion to the most utilized 3 Rs, omitting redistribution due to lack of dedicated imaging.

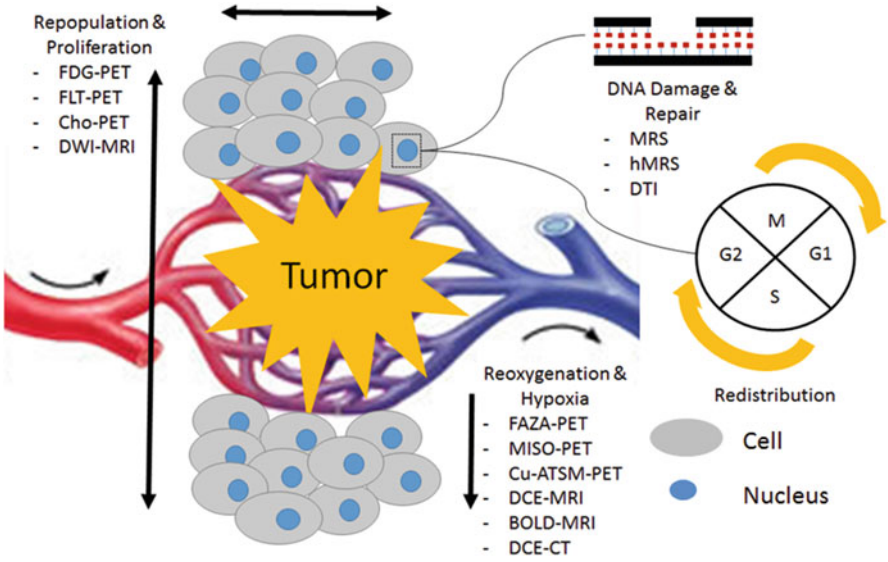

Fig. 9.2 Schematic representation of the 4 Rs of radiotherapy

Repopulation: Metabolism and Proliferation

The malignant transformation of normal tissues and the subsequent growth of new neoplasms rely on a host of molecular changes that lead to the acquisition of pro-growth capabilities, including (but not limited to) self-sufficiency in growth factors, insensitivity to antigrowth signals, limitless proliferative potential, sustained angiogenesis, and evasion of apoptosis [8]. A growing tumor is often first detected clinically (or with planned radiographic screening) as a growing mass, representing an underlying abnormal proliferation of cells. This represents the standard target of radiotherapy and is delineated in an anatomical fashion on CT or MRI. Functional imagining provides an opportunity to evaluate the underlying molecular signatures of cancer growth, to potentially aid in targeting, adaptation, and assessment of treatment response.

Glycolysis

Glycolysis is the cellular conversion of glucose to energy, a process that is upregulated in the proliferative atmosphere of malignancy. Currently, the most heavily utilized functional imaging modality in cancer care exploits this phenomenon by modifying a glucose molecule to contain a positron-emitting fluorine-18 isotope, namely, fluorodeoxyglucose (FDG). FDG-based positron-emission tomography

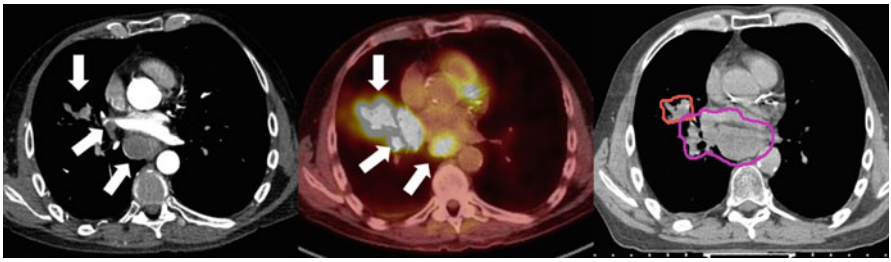

Fig. 9.3 Baseline CT (*left*), FDG-PET (*middle*), and planning CT (*right*) images of a patient with stage IIIA (T2N2) lung adenocarcinoma treated with concurrent chemoradiation. *White arrows* denote the primary tumor and nodal disease on CT and FDG-PET images; the *solid lines* delineate the radiotherapy targets, primary (red) and nodal (magenta) internal target volumes, respectively

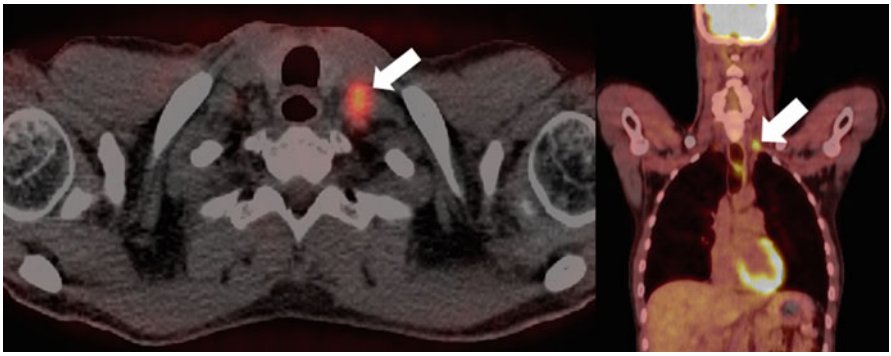

Fig. 9.4 Baseline axial and coronal FDG-PET images of a patient with squamous cell carcinoma of the upper thoracic esophagus. The FDG-PET scan identified a supraclavicular node (*white arrows*) that was subsequently included in the radiation treatment volume

(PET) is able to image the differential uptake of glucose in tumor cells over neighboring normal cells owing in part to their higher metabolic requirements. The common measurement used in PET is the standard uptake value (SUV), defined as voxel activity per dose injected per body mass. FDG-PET has been shown to be extremely powerful in identifying cancer cells, even in the absence of abnormal anatomic morphology. The combination of PET with CT has resulted in vastly improved sensitivity in detecting occult disease missed by CT, resulting in improved locoregional targeting and where appropriate omitting intensive curative treatments in patients with distant metastasis. In non-small cell lung cancer (NSCLC) (Fig. 9.3), the addition of FDG-PET to conventional staging assessment has shown a change in planned management in 20–30 % of patients, mainly in reducing the number of futile thoracotomies [9]. Similarly in esophageal cancer (Fig. 9.4), FDG-PET has been found to improve the sensitivity for detection of metastatic disease by up to 20 % over CT alone [10]. In head and neck cancers, the use of FDG-PET/CT has become common due to the high sensitivity, specificity, and accuracy for metastatic disease (>75 %) [11] and the finding that local radiotherapy plans changed from curative to palliative

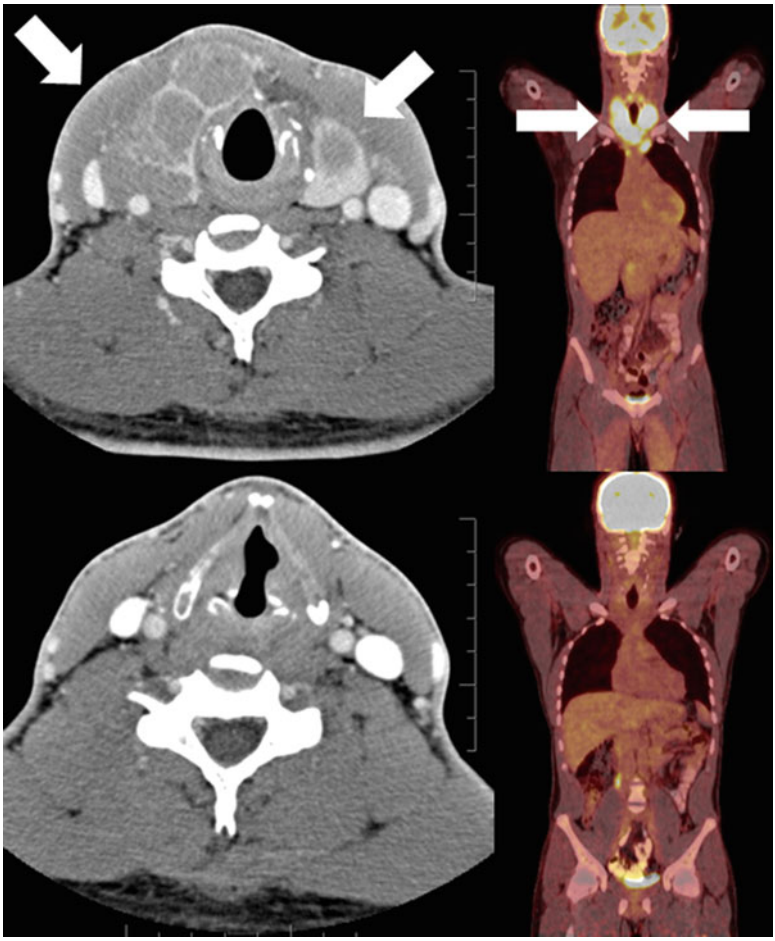

Fig. 9.5 CT (*left*) and FDG-PET (*right*) images of a patient with stage IIA_X Hodgkin's lymphoma at baseline (*top*) and after the planned four cycles of combination chemotherapy and involved field radiotherapy (*bottom*). *White arrows* denote the tumor at baseline. The patient achieved complete CT and metabolic response posttreatment

intent in 13 % of patients when FDG-PET information was added [12]. FDG-PET has also had a large impact in the care of lymphoma patients, particularly those with Hodgkin's lymphoma (HL) (Fig. 9.5). Staging FDG-PET results in stage migration in ~25 % of patients with HL and a change in management in up to 15 % [13]. The standard of care for numerous malignancies now involves FDG-PET/CT in the work-up, including the lung and lymphoma to name a few.

The rise in utilization of FDG-PET as a staging investigation has led investigators to study its use as a quantitative biomarker via the SUV measurement. In an examination of patients from three prospective clinical trials evaluating chemoradiation in non-operable stage II and stage III NSCLC patients, baseline FDG-PET information

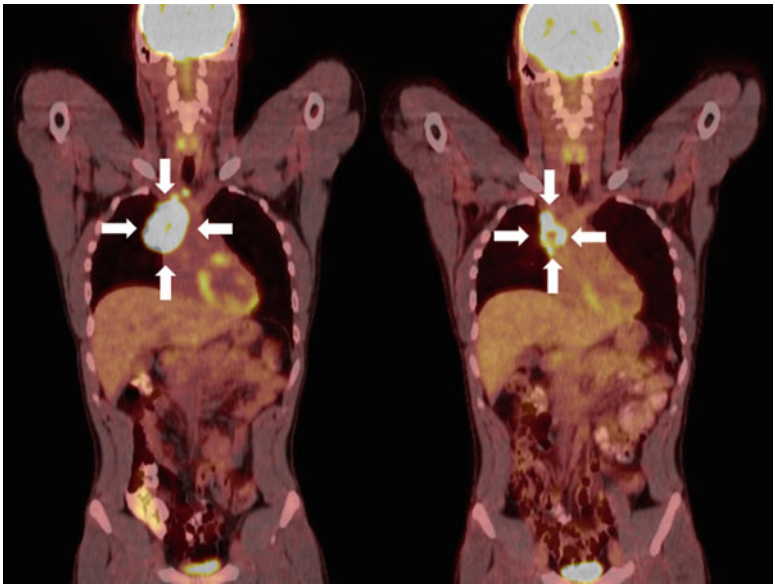

Fig. 9.6 FDG-PET scan images from baseline (*left*) and after six cycles of combination chemotherapy (*right*) of a patient with primary mediastinal diffuse large B-cell lymphoma. *White arrows* denote areas of metabolically active disease. This patient received 35 Gy in 20 fractions of involved field radiotherapy to the areas of persistent FDG uptake

was found to be predictive of local recurrence [14, 15]. Volumes generated by delineating the 70% of pretreatment SUV_{max} were well correlated with the 90% SUV_{max} recurrence volume.

Similar results have been demonstrated in cancers of the head and neck, which have shown that local recurrences are more likely to occur within FDG-avid areas and that the degree and volume of avidity is associated with both local and distant recurrence rates [16, 17]. Furthermore, analogous studies have been conducted with the addition of interim FDG-PET analysis partway through definitive head and neck radiotherapy and have demonstrated that the lack of FDG response is associated with inferior outcome [18]. Studies done in esophageal and rectal cancer are consistent, showing that the degree of metabolic response between pre- and posttreatment scans is associated with outcome [19, 20]. Adaptive PET-guided strategies have been investigated in Hodgkin's and non-Hodgkin's lymphoma alike (Fig. 9.6). In advanced-stage Hodgkin's lymphoma, treatment with six cycles of BEACOPP (escalated) followed by PET-guided radiotherapy resulted in better freedom from treatment failure and less toxicity compared to eight cycles of the same chemotherapy regimen [21]. However, interim analysis of HD10 trial showed that omitting radiotherapy in patients with stage I/stage II Hodgkin's lymphoma who attained a negative early PET scan after two cycles of chemo was associated with an increased risk of early relapse compared to standard combined modality treatment [22].

The linkage with CT has enabled PET to easily integrate into the radiotherapy workflow, and given its promise as a biomarker, the natural extension has been to utilize the combined information directly in radiotherapy planning. The obvious benefit is to identify areas that may be missed on a standard planning CT due to normal anatomic morphology but identified via FDG avidity. Not surprisingly, numerous studies have shown the alteration of final GTV volumes with the inclusion of FDG-PET information [23–26]. FDG-PET has been shown to be the most accurate modality for delineating GTV compared to MRI and CT in pharyngolaryngeal cancer when validated against surgical specimen [27]. Studies are now being conducted to evaluate the benefit of taking this biologic information further by assessing its use as a target for dose painting. As mentioned above, studies have suggested that local glycolytic activity may correlate with resistant disease and therefore a target for dose escalation. Early dose painting studies have established the feasibility of this technique for numerous sites, including the head and neck, lung, and esophagus. Madani et al. showed the safety of dose painting by numbers in a phase I study evaluating the head and neck (non-nasopharynx) of patients undergoing definitive radiotherapy [28]. They showed that a median CTV dose of 80.9 Gy was safely achievable. Similarly, Yu et al. demonstrated a sub-GTV volume based on the pretreatment $SUV_{50\%Max}$ in patients with an SCC of the esophagus could be safely escalated to 70 Gy using a simultaneous integrated boost [29]. In NSCLC, studies integrating FDG-PET into the RT planning process have shown that one can modulate the OAR to CTV dose ratio using metabolic guidance to either shrink boost volumes while keeping overall integral target doses constant (resulting in lower surrounding OAR doses) or conversely by maintaining an iso-OAR dose and dose painting nearby target subvolumes. Van Der Wel et al. showed that when using a prescription dose of 60 Gy, an FDG-PET-based plan could be implemented to reduce the mean esophagus dose from 29.8 to 23.7 Gy and the average lung dose by 2 %. Conversely, for an iso-OAR dose, the mean target dose could be increased to 71 Gy [30]. A phase II study by the Belderbos group showed that the utilization of FDG-PET in planning could be used to safely boost the mean target dose to 77 Gy [31]. Table 9.1 highlights several studies investigating the integration of FDG-PET into the radiotherapy process. For a more dedicated review, please refer to excellent summaries provided by Jelercic and Shi, respectively [23, 32]. Prospective studies are now being developed to test whether these modifications can result in meaningful clinical endpoints, including RTOG-1106 investigating whether FDG-PET-guided radiotherapy can improve local control in stage III NSCLC (RTOG-1106).

In addition to the value of metabolic imaging at baseline, the ability to compare glycolytic activity following treatment has been shown to offer independent prognostic information. In cancers of the head and neck, FDG-PET acquired 24-week post-treatment demonstrated >90 % sensitivity and specificity in locating recurrent disease and offered an 85 % rate of concurrent targeted biopsies [33]. In locally advanced esophageal cancers, Kauppi et al. demonstrated that percentage change in SUV of the primary tumor (pre- and post-neoadjuvant chemotherapy) was independently predictive of overall survival (HR 0.966 per 1 % increase, $p<0.0001$) [34]. FDG-PET response has been correlated pathologically by Bahace et al., investigating patients with superior sulcus tumors who underwent trimodality therapy and demonstrating

Table 9.1 Summary of select studies utilizing FDG-PET in tumors treated with radiotherapy

Reference	Study type	Tumor site	*N*	Findings
Calais et al. [14]	Prospective	NSCLC	39	70 % SUV_{max}-threshold subvolumes at baseline correlate with 90 % SUV_{max}-threshold volume at relapse (>0.51 common volume/recurrent volume)
Bradley et al. [15]	Prospective	NSCLC	26	Integration of FDG-PET resulted in a GTV contour change in 58 % of patients, in 12 % the volume decreased due to improved ability to delineate in atelectatic lung, and 46 % the volume increased due to additional tumor detected
Roh et al. [16]	Retrospective	Hypopharynx	78	Increased metabolic tumor volume (delineated as isocontour of SUV >2.5) was associated with inferior 4-year overall survival (HR 2.66, $p=0.002$)
Due et al. [17]	Retrospective	HNSCC	520	Most recurrences occur within FDG-avid areas. Recurrence density increased with % SUV isocontour delineation and was highest for 90 % SUV_{max} ($p=0.036$)
Kilic et al. [24]	Retrospective	Rectum	20	CTV targets derived with FDG-PET/CT were significantly larger than CT alone (median CTV volume 559.73 mm^3 vs. 468.43 cm^3, $P=0.043$)
Nkhali et al. [26]	Retrospective (planning study)	Esophagus	10	The median GTV volume delineated at baseline and again after 37.8–42 Gy (+ concurrent cisplatin) using FDG-PET decreased from 12.9 to 5.0 cm^3 ($p=0.01$), resulting in a significant reduction in the lung V_{20} (26.8–23.2 %, $p=0.006$)
Madani et al. [28]	Prospective	HNSCC	39	Phase I study showing FDG-based dose painting by numbers allowed dose escalation to a median 80.9 Gy, with no acute grade 3 toxicity and only one patient with grade 2 toxicity (mucosal ulceration). One-year local control was 87 %
Yu et al. [29]	Prospective	Esophagus	25	Dose escalation to a subvolume (50 % SUV_{max} isocontour) to 70 Gy in 2.8 Gy fractions using simultaneous integrated boost, and concurrent chemotherapy was achievable with two grade 3 toxicities (one myelosuppression, one nausea/vomiting). One-year local control was 77.4 %
van Elmpt et al. [31]	Prospective	NSCLC	20	Dose escalation to a metabolic tumor volume (50 % SUV_{max}) was achievable to ≥72 Gy in 15/20 (75 %) patients while maintaining planning OAR constraints

Abbreviations: *CTV* clinical target volume, *FDG* fluorodeoxyglucose, *GTV* gross tumor volume, *HNSCC* head and neck squamous cell carcinoma, *NSCLC* non-small cell lung cancer, *OAR* organ(s) at risk, *PET* positron emission tomography, *SUV* standardized uptake value

that the maximum SUV obtained following chemoradiotherapy was correlated with the amount of remaining viable tumor cells ($R=0.55$, $p=0.007$) [35]. In squamous cell carcinomas of the cervix, Schwarz et al. showed that FDG-PET images acquired 3 months post chemoradiotherapy were predictive of the response. Twenty-three percent of patients with complete metabolic response experienced treatment failure, compared to 100 % of those with progressive metabolic activity and 65 % of those with partial metabolic response [36]. These results emphasize the role of FDG-PET in oncology, and particularly radiotherapy, further accentuating the importance of prospective studies integrating this information into treatment planning as discussed above.

Proliferation

The ability of tumor cells to divide and grow in a self-sustained fashion is one of the hallmarks of cancer; it has been shown that the rate of proliferation is prognostic in many cancers in many sites [37–40]. Additionally, the rate of tumor growth can increase after treatment (chemotherapy or radiotherapy), a phenomenon named "accelerated repopulation" [41]. Numerous disease sites have demonstrated a reduced rate of local control with prolonged treatment courses, highlighting the importance of this effect [42–46]. The ability to identify a tumor's specific proliferative potential at the outset of treatment and then follow dynamic changes during/after treatment may be beneficial in modern radiotherapy.

PET

The functional imaging tracer, 3′-deoxy-3′-^{18}F-fluorothymidine (FLT), has been proposed as a noninvasive imaging biomarker for proliferation based on its biochemical pathway in dividing cells. FLT is taken up by cells and is phosphorylated by thymidine kinase-1 (TK1), trapping it within the cell (Fig. 9.7). TK1 is upregulated in S-phase and is thus an indirect measurement of cell division. FLT uptake has been shown to correlate with the gold standard in pathologic proliferative status, Ki67, in a number of cancer sites, and in and of itself has shown to be a prognostic biomarker based on treatment response [47–49]. In squamous cell cancers of the head and neck, a decrease in FLT uptake (SUV_{max} and PET-segmented GTV) during the first 2 weeks of definitive radiotherapy (± chemotherapy) was associated with better 3-year disease-free survival (88 % vs. 63 %, $P=0.035$, and 91 % vs. 65 %, $P=0.037$, respectively) [50]. The use of FLT imaging has been extensively investigated in terms of targeted growth signal modifiers, most commonly modulators of the epidermal growth factor receptor (EGFR). One study showed that early changes in FLT-PET during the first week erlotinib treatment predicted significantly longer progression-free survival (HR 0.3) in patients with NSCLC [51]. Furthermore, FLT has been shown to be a better marker of disease response than FDG-PET during radical chemoradiation, although the results are still pending on if this will translate to a difference in patient outcome in a prospective setting [52].

Fig. 9.7 Baseline CT (*left*), FDG-PET (*middle*), and FLT-PET (*right*) images of a patient with newly diagnosed non-small cell lung cancer. The *thick white arrow* indicates the primary tumor. The *thin white arrow* represents a mediastinal lymph node that is avid on FLT-PET scan, but not on the corresponding FDG-PET scan (courtesy of Dr. Meredith Giuliani)

Similar to FDG-PET, FLT-PET is commonly integrated with CT scanning, providing a relatively straightforward integration into the radiotherapy pathway. Planning studies investigating this integration have provided promising preliminary results. In thoracic esophageal cancers, the GTV volumes constructed using FLT-based parameters were generally 10% smaller than anatomic delineations, resulting in a 10% reduction in mean lung and heart doses ($p<0.01$) and showed higher correlation with final pathologic size [53]. Planning studies have also shown the feasibility of boosting areas of high proliferation in tumors of the oropharynx and rectum [54, 55]. A comprehensive review focused on FLT in oncology is provided by Tehrani et al. [56].

Choline is a substrate for synthesis of phosphatidylcholine, which is a major component of the cellular membrane. Choline can be tagged with a carbon-11 or fluorine-18 positron-emitting radionuclide for use in PET scanning (Cho-PET). With cellular turnover elevated in malignancies, accumulation of choline can be demonstrated in areas of active disease. Cho-PET has been most heavily investigated in prostate cancer and has shown improved sensitivity and specificity for both regional and distant disease detection over conventional staging modalities [57]. Cho-PET has also been investigated in regard to identifying dominant tumor nodules within an intact prostate, possibly for local dose escalation strategies. Currently the standard imaging for this task is multi-parametric MRI (mpMRI). However, a meta-analysis by Chan et al. showed that while Cho-PET alone was roughly equivalent to mpMRI in identifying a dominant nodule, the combination of both had improved sensitivity and specificity over either alone [58]. Planning studies using Cho-PET for defining subvolumes for dose escalation up to 90 Gy have shown gains in estimated tumor control probability (TCP) without exceeding OAR tolerances [59, 60]. Pinkawa et al. implemented this technique up to 80 Gy and showed no adverse effects on toxicity or quality of life [61]. The utilization of Cho-PET has been more widely accepted in the setting of recurrent disease and now represents the standard of care in many countries, including the United States, for restaging prior to definitive salvage treatment [62]. There is single institution data supporting the feasibility of Cho-PET-directed salvage treatment up to 74 Gy; however larger series and longer-term outcomes are needed [63]. Table 9.2 provides a summary of relevant literature pertaining to radiotherapy and proliferative imaging modalities.

Table 9.2 Summary of select studies utilizing FLT and choline PET in tumors treated with radiotherapy

Reference	Tracer	Study type	Tumor site	*N*	Findings
Hoeben et al. [50]	FLT	Retrospective	HNSCC	48	A relative change in tumor $SUV_{max} \geq 45\,\%$ from baseline to after 1.5 weeks of treatment (median 14 Gy, range 10–24 Gy) was associated with improved disease-free survival (88 % vs. 63 %, $p = 0.035$)
Everitt et al. [52]	FLT	Prospective	NSCLC	20	Visual analysis of both FLT and FDG PET after 2 weeks of CRT (compared to baseline) showed that 52 % of patients had a partial metabolic response, while 76 % had a partial proliferative response, suggesting earlier tumor cell proliferation is affected more rapidly than metabolism
Troost et al. [55]	FLT	Prospective	HNSCC	10	A significant decrease in SUV_{max} was seen during radiotherapy (compared to baseline), greatest after 2 weeks of treatment (20 Gy), but continuing through 4 (40 Gy) weeks of treatment (7.6 vs. 3.1 vs. 1.7, $p = 0.0001$ and 0.001, respectively)
Chang et al. [59]	Cho	Prospective (planning study)	Prostate	8	A SIB to 90 Gy to a subvolume defined by 70 % SUV_{max} threshold resulted in a higher TCP across all patients (mean increase 37 %, $p < 0.001$) with no significant change in NTCP rectum and bladder
Pinkawa et al. [61]	Cho	Prospective	Prostate	67	Delivery of a SIB to 80 Gy to a subvolume defined by a tumor-to-background ratio >2 did not result in significantly increased acute or late bladder/bowel toxicity or decreased QoL (median 2 and 19 months post-RT) compared to a similar cohort not treated with SIB

Cho choline, *CRT* chemoradiotherapy, *FDG* fluorodeoxyglucose, *FLT* 3′-deoxy-3′-^{18}F-fluorothymidine, *HNSCC* head and neck squamous cell carcinoma, *NSCLC* non-small cell lung cancer, *NTCP* normal tissue complication probability, *PET* positron emission tomography, *QoL* quality of life, *RT* radiotherapy, *SIB* simultaneous integrated boost, *SUV* standardized uptake value, *TCP* tumor control probability

Diffusion-Weighted MRI

MR diffusion imaging is an imaging sequence based on the thermally driven random motion of water molecules (Brownian motion). By applying strong gradient pulses, local diffusivity can be measured, and regions can vary depending on the local

microenvironment. Generally, higher cellular density equates to lower diffusivity [64]. The metric generally used to quantify this diffusivity within a given volume element is referred to as the apparent diffusion coefficient (ADC), given in units of area/time. The term "apparent" is used because true diffusion is affected by innumerable variables which cannot be individually quantified in-situ (i.e., intravoxel motion, microvascular perfusion, physical obstacles within the cell, etc). Lower ADC values represent more restricted diffusion (Fig. 9.8); it has been reported across numerous sites that regions of malignancy have lower ADC values than surrounding healthy tissue [65–68]. Intuitively, regions of increased proliferation lead to areas of increased cellularity; and ADC has also been shown to correlate with Ki67 in both bladder and breast cancer [69, 70]. Furthermore, areas of reduced ADC have been shown to be associated with higher grades of breast, bladder, endometrial, and prostate cancer [69, 71–73]. The use of DWI in the identification of high-grade prostate cancer has been particularly useful and relevant for management decisions and now features prominently in the prostate imaging reporting and data system (PI-RADS) classification system for MRI evaluation of prostate cancer [74]. In a recent review by Futterer et al., DWI was able to provide a negative predictive value of up to 98 % for the presence of greater than Gleason 6 prostate cancer [75]. Baseline ADC values have also been shown to be biomarkers of disease-free survival in patients undergoing radical chemoradiation for squamous cell carcinomas of the cervix. A retrospective study by

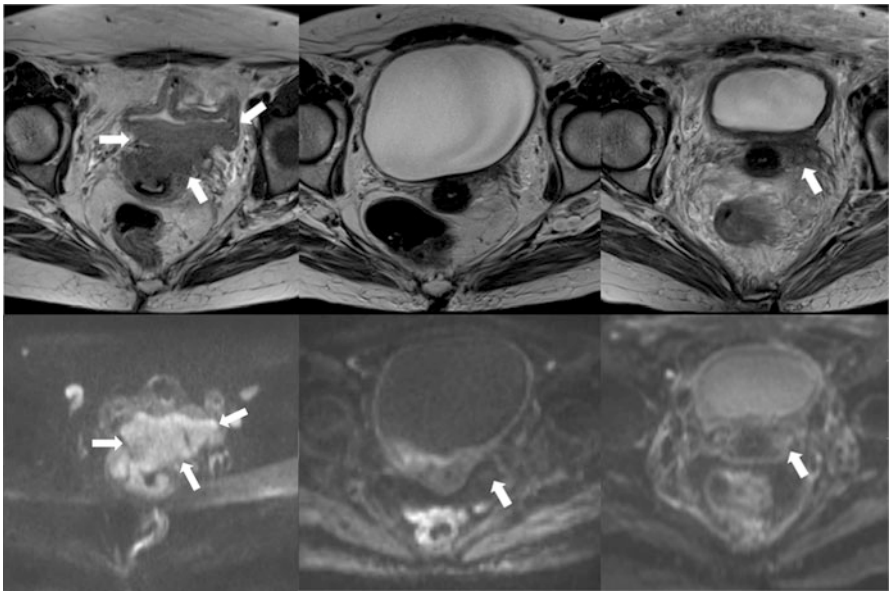

Fig. 9.8 Axial MRI images acquired pretreatment (*left*), 3 months after completion of chemoradiation (*mid*) and at the time of recurrence 1 year post-chemoradiation (*right*) in a woman who presented with stage IVA cervical squamous cell carcinoma. Along the top are T2-weighted images, and below are the corresponding diffusion-weighted images ($b = 800$ s/mm^2). *White arrows* denote initial disease and the area of recurrence. Note the persistent restricted diffusion even at time of radiographic complete response posttreatment

Micco et al. demonstrated that a higher pretreatment mean tumor ADC was associated with better disease-free and overall survival in patients treated with chemoradiation on univariate analysis (HR 0.56, $p=0.007$; HR 0.46, $p=0.02$) [76]. Similar findings were reported by other groups investigating cervical cancer [77, 78]. In postoperative recurrences of cervical cancer, a tumor ADC $>0.95\times10^{-3}$ mm^2/s was predictive of a lack of complete response to chemoradiation in bulky lesions (sensitivity 85.7%; specificity 100%, $p=0.05$) [79]. In rectal cancer, a systemic review showed that pretreatment ADC was predictive of pCR following neoadjuvant chemoradiation with a negative predictive value of 90% and a specificity of 68% [80].

Much like FLT imaging, DWI-MRI has shown promise in measuring the dynamic changes of malignancies throughout and after treatment, offering an in vivo barometer of treatment effect. The hypothesis is that treatment-induced cell death will result in lower cellular density, reducing the restrictions to intercellular water diffusion and therefore increasing local ADC. Unlike single pretreatment measurements, increasing ΔADC with treatment (ADC_{post}–ADC_{pre}) has consistently shown positive associations with outcome. A work by Yu et al. demonstrated that patients treated with stereotactic radiotherapy for hepatocellular carcinoma with an increment of ≥20% in ADC value (6 months vs. pretreatment) had significantly better local progression-free survival at 1 year [81]. Greater increases in tumor ADC early (mostly 1–3 weeks) during RT ± concurrent chemotherapy have been associated with better response in many cancers: high-grade glioma [82], head and neck squamous cell carcinoma [83], nasopharynx cancer [84], liver tumor (hepatocellular carcinoma, liver metastases, cholangiocarcinoma) [85], rectal cancer [86–88], and cervix cancer [89–91]. In particular, a meta-analysis done by Fu et al. demonstrated a significant association between ΔADC and the status of residual tumor post-chemoradiation in locally advanced cervical cancer patients ($p<0.001$), suggesting its utility in monitoring treatment response [92]. There is currently limited work investigating the real-time integration of DWI-MRI directly into radiotherapy planning, but preliminary work does show promise [93–95]. Table 9.3 provides a representative summary of evidence investigating DWI-MRI in conjunction with radiotherapy.

Summary

A trait common to many malignancies is the increase in cellular proliferation, which can manifest as local increases in glycolysis and cellular density. Novel functional imaging modalities have probed each of these facets directly, including quantifying FDG uptake with PET, assessing cellular density with DWI-MRI, and directly estimating local proliferation rates with FLT-PET. Each of these modalities has been shown to be useful in oncologic imaging and have been investigated to improve staging. Each is increasingly showing promise as a quantitative peri-treatment biomarker for treatment response and/or long-term outcome. Retrospective studies have shown benefit with integration into radiotherapy planning/dose painting, and larger prospective trials are now ongoing.

Table 9.3 Representative summary of literature investigating DWI-MRI utility in radiotherapy

Reference	Study type	Tumor site	Timing of DWI	*N*	Findings
Micco et al. [76]	Retrospective	Cervix	Pretreatment	49	Decreased baseline mean tumor ADC was associated with inferior DFS and OS on univariate analysis (HR 0.56, $p=0.007$, and HR 0.46, $p=0.02$, respectively)
Nakamura et al. [77]	Retrospective	Cervix	Pretreatment	80	Decreased baseline mean tumor ADC was associated with inferior DFS on multivariate analysis (HR 4.11, $p=0.013$)
Chopra et al. [79]	Prospective	Cervix (recurrent)	Pretreatment	20	Mean tumor ADC $>1.0\times10^{-3}$ mm^2/s was predictive of partial response to CRT (sensitivity 85.7 %; specificity 100 %, AUC = 0.96, $p=0.05$). Of nine partial responders, three had residual disease spatially corresponding to baseline area of restricted diffusion
Joye et al. [80]	Meta-analysis	Rectal	Pre- and posttreatment	226	A decreased baseline tumor ADC and increased ΔADC (pre–post was predictive of pCR following neoadjuvant chemoradiation-NPV 90 %, PPV 35 %; and NPV 94 %, PPV 46 %, respectively)
Yu et al. [81]	Retrospective	HCC	Pre- and posttreatment	48	ΔADC [(pre–post)/pre] >20 % was associated with better 1-year local control (100 % vs. 75.8 %, $p=0.02$). Post-treatment scans were taken 3–5 months following SBRT (15–20 Gy/3 fractions)
Hamstra et al. [82]	Prospective	High-grade glioma	Pre-, mid-, and posttreatment	60	Patients with an increase in ADC in >4.7 % of voxels within the GTV after 3 weeks of RT (30 ± 4 Gy) had longer median survival (52.6 months vs. 10.9 months, $p<0.003$)
Galban et al. [83]	Prospective	HNSCC	Pre- and mid-treatment	15	The mean whole tumor ADC after 3 weeks of CRT was significantly higher in patients with radiographic CR than in those with PR (0.0016 mm^2/s vs. 0.0014 mm^2/s, $p<0.05$)
Chen et al. [84]	Prospective	Nasopharynx	Pre-, mid-, and posttreatment	31	ΔADC (mid-pre and post-pre) of both primary tumor and metastatic lymph nodes was significantly higher in patients with CR than those with residual disease ($p \leq 0.05$)
Fu et al. [92]	Meta-analysis	Cervix	Pre- and posttreatment	577	Post-treatment ADC was significantly higher than pretreatment ADC in patients treated with CRT (standardized mean difference 2.95 mm^2/s, 95 % CI 2.19–3.72, $p<0.001$)

ADC apparent diffusion coefficient, *CRT* chemoradiotherapy, *DFS* disease-free survival, *HCC* hepatocellular carcinoma, *HNSCC* head and neck squamous cell carcinoma, *OS* overall survival, *pCR* pathological complete response, *SBRT* stereotactic body radiotherapy

Reoxygenation: Hypoxia and Vascularization

Hypoxia refers to the phenomenon where cells are deprived of oxygen, which is essential for a variety of cellular functions. A prolonged hypoxic environment leads to changes in cellular metabolism and genomic expression that can result in alterations of glycolysis and DNA repair. Tumor hypoxia is often a result of the rapid proliferation and abnormal vasculature associated with malignant growth. The chaotic and unorganized growth of cancer creates an unpredictable variation of oxygenation among and within tumors. Hypoxic tumors are more resistant to treatment and are associated with poor clinical outcome [96, 97]. There is strong prospective evidence that modification of hypoxia itself leads to improved tumor control [98–100]. With regard to radiotherapy, in particular, the lack of oxygen disrupts one of the major radiobiologic methods of cell killing—free radicals. The deposition of high-energy photons leads to local ionization; the resultant free radicals directly inflict DNA damage. This damage can become permanent with the fixation of nearby oxygen to become stable organic peroxides. In the absence of oxygen, this damage can be repaired more effectively. The gold standard for measuring hypoxia is polarographic electrodes, which can measure oxygen tension directly in the tissue [101, 102]. However, this method requires the invasive introduction of an electrode into the tissue itself; therefore, it is not feasible in many cancer sites. The ability to detect hypoxia noninvasively by imaging enables not only better quantification of tumor heterogeneity but also a potential biologic target for radiotherapy.

PET

A number of positron-emitting tracers have been evaluated for imaging hypoxia. The most prominent probes are nitroimidazole-based, a compound that was first shown by Chapman to remain trapped within hypoxic cells [103]. Among the nitroimidazole-based probes, the most investigated are fluoromisonidazole (FMISO), diacetyl-bis-N4-methylthiosemicarbazone (Cu^{60} or Cu^{64}-ATSM), and fluoroazomycin arabinoside (FAZA) (Fig. 9.9). These probes have shown promise as not only a reliable biomarker of hypoxia but also an association with outcome across many tumor types. Pre-treatment PET imaging of tumor hypoxia in patients with head and neck, lung, brain, and cervical cancers has been shown to correlate with disease-/progression-free survival [104–107], cancer-specific survival [108, 109], and overall survival [110–113] following (chemo)radiation. A meta-analysis by Horsman across multiple tumor types and a variety of tracers showed that hypoxic tumors were more likely to have poor response to radiotherapy (OR 0.27, 95 % CI, 0.18–0.39) [114].

Although a meta-analysis showed that hypoxia-modifying therapies improved locoregional control (HR 0.77; 95 % CI 0.71–0.86) and overall survival (HR 0.87; 95 % CI 0.80–0.95), they have not been adopted in clinical practice because of practical limitations and toxicities [100]. Initial studies looked at ameliorating the hypoxic environment directly via improving oxygenation (carbogen + nicotinamide), hypoxic

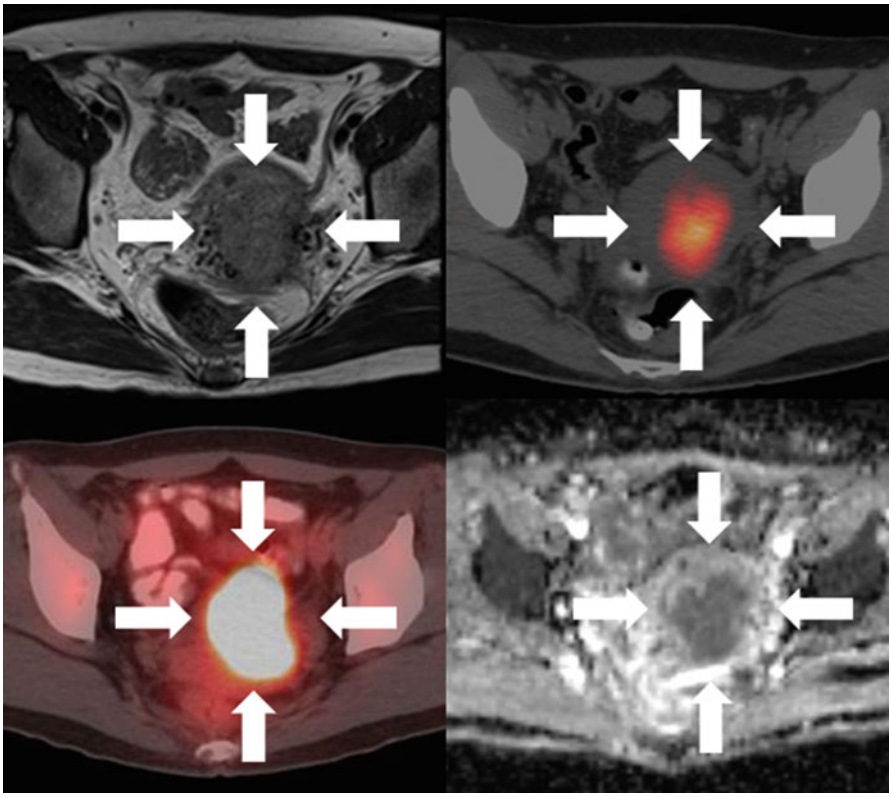

Fig. 9.9 Baseline axial T2 MRI (*left upper*), FAZA-PET/CT (*right upper*), FDG-PET (*left lower*), and ADC map (*right lower*) images of a patient with stage IIIB cervix squamous cell carcinoma. *White arrows* indicate the primary tumor. Note the tumor shows focal FAZA uptake, strong FDG uptake, and restricted diffusion

radiosensitizers (e.g., nimorazole), or direct hypoxic cytotoxins (e.g., tirapazamine). These strategies are not specific to the spatial distribution of hypoxia. Radiotherapy allows for integrated and personalized hypoxia targeting via dose painting. Several dosimetric studies highlighted the feasibility of this approach without excess dose to the OAR. Planning studies in carcinomas of the head and neck using FAZA-PET have shown the ability to dose escalate hypoxic regions in a simultaneous boost up to 86 Gy, without significant effect on existing OAR dose constraints. Specifically, Servagi-Vernat et al. showed that this adaptive FAZA-based dose painting is feasible with FAZA-PET imaging at three time points (baseline, post 7 and 12 fractions), offering the ability to target hypoxic regions dynamically over time [115]. Similarly, dose escalation to hypoxic regions identified by FMISO-PET beyond 80 Gy is feasible without excessive increase of dose to the OARs [116, 117].

An important limitation of dose painting based on hypoxic PET signals is the temporal instability of hypoxia. Radiotherapy based on pretreatment scans inherently assumes a robust target throughout treatment. Various studies have suggested that

this may not be the case in regard to hypoxia, and specifically both acute and chronic hypoxia can be important in radiation resistance. Work by Lin et al. investigated this prospectively in a group of head and neck cancer patients who had consecutive pre-treatment FMISO-PET scans 3 days apart. They found that the mean D95 for the hypoxic GTV was an average of 7 Gy lower (range 3–12 Gy) when the initial plan was applied to the second scan [118]. Bollineni et al. performed serial FAZA-PET imaging in patients with HNSCC and NSCLC and found four cases: (1) increasing hypoxia, (2) decreasing hypoxia, (3) stable hypoxia, and (4) stable non-hypoxia with patients falling into any one of these categories [119]. Further work on the reproducibility, temporal variability, and adapting radiotherapy to hypoxic subvolumes identified by hypoxia tracers is required.

In addition to its *prognostic* value, PET imaging with FAZA can also monitor and/or predict response to hypoxia-targeted therapy. Xenograft studies showed that FAZA tumor uptake declined by 55–70% 1–3 days after administration of BAY 87-2243, a preclinical inhibitor of mitochondrial complex I that decreases tumor hypoxia and sensitizes tumor to radiation [106, 120]. Another xenograft study showed FAZA uptake to predict response to hypoxic cytotoxin tirapazamine and radiation [121]. Table 9.4 provides a representative review of the literature of PET-based hypoxia imaging in conjunction with radiotherapy, and further description of the use of PET-based hypoxia imaging can be found in excellent reviews by Padhani and Fleming [122, 123].

MRI

Several specific MRI sequences have been shown to correlate with tumor hypoxia. Dynamic contrast-enhanced MRI (DCE-MRI) is the most clinically utilized of these. DCE-MRI is a surrogate measurement for hypoxia, as it directly measures vasculature and local disruptions to blood flow. The main principle is to acquire a baseline non-contrast T1-weighted image as a reference set. A gadolinium-based contrast agent is then injected at a known rate and a second set of T1-weighted images is acquired. The contrast is readily seen as an increase in signal and the dynamic change in signal can be quantified. Based on the signal seen outside the vasculature, a parameter called K^{trans}, which represents the "leakiness" of the local vasculature, is modeled. Tumors often have poorly organized and quasi-functional vasculature which can be quantified using DCE-MRI. DCE-MRI has been found to be correlated with oxygen levels measured by polarographic electrodes in cervical cancer [124, 125]. In prostate cancer, hypoxia-inducible factor 2α (HIF-2), a known hypoxia pathway, has been shown to be negatively correlated with the 5th percentile K^{trans} in a histologic comparative study [126]. Similarly, negative correlations with K^{trans} were shown with hypoxic and radioresistant xenografts of cervical carcinoma and primary glioma [127, 128]. Halle et al. combined DCE-MRI data with gene expression profiles of biopsies from patients with cervical cancer treated with definitive chemoradiation [129]. They first identified a DCE parameter called A_{Brix} that had the strongest association with progression-free survival in these patients (in which tumors with

Table 9.4 Summary of select PET-based hypoxia imaging studies in tumors treated with radiotherapy

Reference	Tracer	Study type	Tumor site	*N*	Findings
Mortensen et al. [104]	FAZA	Prospective	HNSCC	40	Significant difference in 2-year DFS between patients with hypoxic tumor at baseline (T/M ≥1.4) vs. non-hypoxic tumor (60 % vs. 93 %, respectively)
Zips et al. [107]	FMISO	Prospective	HNSCC	25	Greater hypoxic volume and tumor-to-background ratio after 1 and 2 weeks of RT were associated with inferior local PFS
Dehdashti et al. [108]	Cu60-ATSM	Prospective	Cervix	38	Significant difference in 3-year PFS between patients with hypoxic tumor (T/M>3.5) vs. normoxic tumor (28 % vs. 71 %, respectively)
Kikuchi et al. [109]	FMISO	Prospective	HNSCC	17	Patients with hypoxic tumors ($SUV_{max} \geq 2.3$ or T/M ≥ 1.3) pre-RT had lower local control rates
Spence et al. [113]	FMISO	Prospective	GBM	22	Increasing hypoxic subvolumes of tumor (number of voxels with T/B > 1.2) and maximum T/B value were each independently associated with inferior OS following CRT (log HR 0.05; 1.57, respectively, $p<0.05$)
Servagi-Vernat et al. [115]	FAZA	Retrospective (planning study)	HNSCC	12	Hypoxic subvolumes within the GTV ($SUV_{tumor} > 3\sigma * SUV_{muscle}$) could be safely boosted to 86 Gy without violating OAR tolerances
Chang et al. [116]	FMISO	Retrospective (planning study)	HNSCC	8	A mean increase in TCP of 20 % could be achieved by targeting hypoxic subvolumes (T/M>1.5) to 84 Gy (compared to 70 Gy plan). The 84 Gy plan increased the mean parotid and mandible NTCP by 18 % and 25 %, respectively, although the differences were not statistically significant
Henriques de Figueiredo et al. [117]	FMISO	Retrospective (planning study)	HNSCC	10	Dose escalation to a hypoxic target volume (automatic segmentation based on adaptive Bayesian method) (79.8 Gy from 70 Gy standard plan) led to a mean increase in TCP of 18.1 % with a mean increase in parotid NTCP of 4.6 %

Cu60-ATSM diacetyl-bis-N4-methylthiosemicarbazone, *DFS* disease-free survival, *FAZA* fluoroazomycin arabinoside, *FMISO* fluoromisonidazole, *GBM* glioblastoma multiforme, *HNSCC* head and neck squamous cell carcinoma, *NSCLC* non-small cell lung cancer, *NTCP* normal tissue complication probability, *PFS* progression-free survival, *RT* radiotherapy, *SIB* simultaneous integrated boost, *T/B* tumor-to-blood ratio, *TCP* tumor control probability, *T/M* tumor-to-muscle ratio, *SUV* standardized uptake value

low A_{Brix} appeared to be most aggressive) [129]. They then found that low A_{Brix} was associated with the upregulation of hypoxia response genes and HIF1α protein and constructed a DCE-MRI signature with the most important genes reflected by A_{Brix}. This DCE-MRI hypoxia gene signature was independently associated with progression-free survival and locoregional control (RR 2.5, 95 % CI 1.3–4.8, and RR 3.7, 95 % CI 1.2–11.8) [129]. Integration of DCE-MRI into the radiotherapy workflow is becoming more feasible with the increasing availability of MRI and specifically MRI simulators within radiotherapy departments. In cervical cancer, the quantity of low-enhancement (i.e., poorly vascularized, likely hypoxic) tumor regions predicted subsequent tumor recurrence [130] and persistently low perfusion from the pre-RT through mid-RT phase independently correlated with inferior local control and disease-free and overall survival [131]. This suggests a potential role for biologic targeting and possible dose escalation; however, prospective studies are warranted. Early planning studies in prostate cancer have demonstrated the feasibility of an integrated boosts to DCE-defined targets to 90 Gy [132]. This has led to several phase 2 studies demonstrating that this strategy can be implemented safely, and now we await the results of a recently completed phase 3 randomized controlled trials investigating the impact on clinical outcome [133, 134].

Another functional MRI technique aimed at measuring in vivo oxygenation is blood–oxygen-level-dependent contrast imaging (BOLD-MRI). Initially developed as a tool for functional brain imaging, this technique is based on the varying magnetic susceptibility of hemoglobin due to oxygenation status. An advantage of this technique is the lack of contrast required for quantification. It was found to correctly predict treatment response to hypoxia-modifying agents in various rodent models [135, 136]. Pathologic correlative studies showed that BOLD-MRI parameters are correlated with HIF-1α staining in both invasive breast cancer and high-grade glioma [137, 138]. Similarly, in prostate cancer, BOLD-MRI findings correlated hypoxia measurements using polarographic electrodes [139]. Investigations of BOLD-MRI directly within the radiotherapy workflow have not yet been done and remain an intriguing avenue for research.

Similar to PET-based hypoxia imaging, temporal uncertainties are present in MRI-based modalities. A planning study by Sovik et al. on canine sarcomas showed that plan adaptation based on hypoxic subvolumes defined by DCE-MRI improved the tumor control probability by 20 %, if replanned twice a week as compared to a single baseline acquisition [140]. Dedicated studies investigating the temporal uncertainties of tumor hypoxia imaged via BOLD-MRI are required. A recent review of MRI-based hypoxia imaging in cancer is provided by Matsuo [141].

CT

Analogous to DCE-MRI is perfusion-based computed tomography, DCE-CT. Based on a similar acquisition but with iodinated rather than gadolinium-based contrast media, DCE-CT quantifies comparable modeling parameters. Again these parameters

are linked to tumor vasculature and have been shown to be a useful surrogate for hypoxia. In NSCLC, DCE-CT derived tumoral blood volume is negatively correlated with histologically based hypoxia via pimonidazole staining [142]. Similarly, in head and neck cancers, tumor hypoxia is correlated with DCE-CT parameters, although not as strongly as with DCE-MRI [143]. Prospective studies investigating the role of anti-angiogenic therapy in head and neck cancers have demonstrated a decline in tumor blood flow and CT enhancement with DCE-CT post-treatment [144]. In high-grade glioma, serial postoperative DCE-CT in patients treated with combined chemoradiation demonstrated a negative correlation between tumor blood flow and blood volume in the residual tumor with survival [145]. As with PET-CT, DCE-CT presents a promising candidate for integration into the radiotherapy workflow, perhaps even more so given the ability to obtain scans directly on a standard CT simulator (with appropriate post-acquisition processing). Future dosimetric and clinical studies integrating DCE-CT are needed. Review articles highlighting the role of DCE-CT in radiotherapy are provided by van Elmpt and Astner et al. [146, 147].

Summary

Hypoxia has been well established as a negative predictive feature in oncology and specifically has been associated with radioresistance. The identification and quantification of tumor hypoxia offers a chance to customize treatment and/or subsequent clinical follow-up. Radiographic biomarkers offer the ability to quantify hypoxia in sites not amenable to direct measurement and also allow measurements in a fully geometric and temporal manner. The integration of these imaging modalities into the radiotherapy workflow has the potential to facilitate hypoxia-directed dose painting, adaptation, and personalized follow-up. Further prospective work is required to fully elucidate the clinical benefit of such a strategy.

Repair

Radiotherapy inflicts DNA damage, and ultimately cell killing, by a process of breaking base-pair linkages via ionization. The cellular response to this assault is to initiate DNA repair via one of several pathways (e.g., homologous repair, nonhomologous end joining, base excision repair, etc.) [148]. Due to the scale, the repair itself cannot be directly visualized; however, surrogates have been developed to provide macroscopic insight into this process. The obvious goal of radiotherapy is to minimize tumor repair and maximize normal healthy tissue repair, and the most direct route is by shaping target and avoidance doses, respectively. The potential for measuring repair in vivo represents an intriguing adjunct to this strategy. Not only does it represent an independent marker for delineation, as often the repair mechanisms differ between tumor and normal tissues, but there is potential for measuring

the local repair efficiency within each, enabling targeting of high repair regions of tumor and avoiding poorly repairing healthy structures [149]. Doubling down in this manner presents an intriguing tactic for widening the therapeutic window.

Magnetic Resonance Spectroscopy

Magnetic resonance spectroscopy (MRS) is a noninvasive technique to measure metabolite concentrations in the tissue. The principal difference between MRS and anatomic MR measurements is that the signal obtained from hydrogen precession (influenced by neighboring protons) is used to quantify chemical shifts rather than provide contrast information. Another key aspect is to ensure water/fat suppression as these signals would otherwise dominate the observed spectrum. By comparing an acquired shift spectrum against a library of characteristic spectra, various compounds can be identified and their relative concentrations quantified. The most common metabolites that are characterized by MRS are choline (Cho), a component of cellular membranes (increased levels suggest increased cellular turnover), creatine (decreased levels suggest necrosis/cell death), glucose, N-acetyl-aspartate (NAA, a prominent neuronal metabolite reduced in areas of neuronal destruction), and lactate (increased in areas of hypoxia). The most investigated sites utilizing MRS for radiotherapeutic applications are the brain and prostate.

Various studies investigating MRS in gliomas have linked a Cho/NAA ratio >2 (both pre- and postoperatively) with worse outcome [150, 151]. This suggests a potential target for dose escalation, and subsequent planning studies have demonstrated dosimetric feasibility in targeting subvolumes with elevated Cho/NAA ratios up to 72 Gy [152]. A single arm, prospective phase II study of stereotactic boost (15–24 Gy) to regions with an elevated Cho/NAA > 2 (plus standard conformal radiotherapy to 60 Gy) has shown acceptable toxicity and a 6.2-month improvement in median survival versus historical controls, but phase III studies are needed [153]. Furthermore, following completion of adjuvant treatment, a secondary problem of distinguishing residual glioma versus benign regions of necrosis and tissue repair is prevalent. This phenomenon, called pseudoprogression, occurs in ~30 % of patients [154]. Studies have shown MRS as a promising tool in this area, with an elevated Cho/nCho (nCho represents the Cho in the contralateral brain) or Cho/NAA ratio both demonstrating a high specificity for true tumor progression [155, 156]. In a meta-analysis by Zhang et al. evaluating a total of 455 patients with high-grade glioma, an elevated Cho/Cr ratio had a sensitivity and specificity each of 83 % (95 % CI 0.77–0.89 and 0.74–0.90, respectively) for classifying tumor progression [157].

In prostate cells, citrate represents an important metabolite that plays a critical role in metabolism together with zinc ions. High concentrations of citrate are unique to glandular areas of the prostate, which are highest in the peripheral zone. Cancerous prostate cells dedifferentiate and lose the ability to accumulate and secrete citrate, and energy pathways subsequently alter. Elevated citrate/Cho or

citrate/Cr ratios have been shown to be associated with prostate cancer [158]. Targeted biopsies utilizing MRS and MRI guidance have shown a sensitivity, specificity, and accuracy of 100 %, 70.6 %, and 79.2 %, respectively (95 % CI 61.6–100.0, 46.9–86.7, and 57.9–92.9, respectively), in a population of men with a rising PSA and previously negative biopsy [159]. Furthermore, a ratio of choline + creatine + spermine to citrate showed a positive correlation (Spearman's coefficient 0.77, $p < 0.001$) with Gleason score, therefore suggesting an ability to preferentially identify areas of increased aggressiveness [160]. Naturally, this led to planning studies investigating the feasibility of MRS-guided dose escalation, which proved possible up to 90 Gy with EBRT and up to 130 % (~40 Gy) with brachytherapy boost [161, 162]. Limited focal targeting of a dominant intraprostatic lesion, defined by T2W and MRS to 82 Gy and de-escalation of remaining prostate dose to 74 Gy, resulted in a significant rise in TCP (80.1 % vs. 75.3 %, $p < 0.001$) and reduction in rectal normal tissue complication probability (3.84 % vs. 9.7 %, $p = 0.04$) [163]. Prospective studies evaluating the clinical effect of these strategies are lacking.

In addition to standard MRS, hyperpolarized MRS (hMRS) via dynamic nuclear polarization allows for molecules other than hydrogen to be imaged. This can offer advantages in signal-to-noise ratio (as hydrogen is ubiquitous in the body) as well as offer imaging of otherwise low-density areas such as the lungs. One area of interest specific to radiotherapy is the evaluation of radiation-induced lung injury or radiation pneumonitis (RP). Lung doses are often the limiting factor for treatment plans of thoracic based malignancies, particularly lung cancer. This limits the prospects of dose escalation. Carbon-13 is a suitable candidate for hyperpolarization and has been tagged to pyruvate, which converts to lactate, bicarbonate, and alanine upon metabolism. Animal models showed that elevated lactate levels based on C-13 hMRS were associated with RP and were detectable as little as 5 days post-conformal radiotherapy, suggesting a role for early detection and treatment modification in a patient population [164]. Work in hyperpolarized gases (helium-3 and xenon-129) has shown promise as inhaled contrast agents for hMRS, allowing highly detailed ventilation scans, useful for accurately describing a number of lung diseases [165]. Planning studies have suggested that integration of ^{3}He-based hMRS can reduce the volume of ventilated lung that is irradiated, potentially reducing the risk of RP by up to 10 % versus a standard plan [166], and the potential clinical benefit is being assessed in an ongoing randomized controlled trial [167]. A recent review by Nguyen et al. examines the potential role of MRS in modern image-guided radiotherapy [168].

Limitations of spectroscopy are generally related to poor spatial resolution, exacerbated by volume averaging between adjacent voxels. This is accentuated particularly in the era of ever-improving anatomical imaging. Furthermore, inhomogeneities within the magnetic field can result in differences in metabolite quantification, which makes standardization among centers and between individual patients difficult and can limit generalizable protocols.

Diffusion Tensor Imaging

Diffusion tensor imaging (DTI) is a form of DWI that was discussed earlier, but in DTI the directional diffusion is also measured. DWI assesses the Brownian motion of water molecules and quantifies their ability to disperse within a given space. DTI measures this on a directional basis, determining if some paths are more restricted than others. Imagine a garden hose, where water is quite free to "diffuse" longitudinally through the tube, but that flow is significantly attenuated axially by the rubber casing. DTI has been most utilized in brain imaging where neurons are akin to the garden hose in the previous example [169]. Typically a series of DWI images are taken along six different gradient orientations, and diffusion can then be quantified in terms of a vector field rather than a single scalar quantity. Generally, increases in axial diffusivity and decreases in longitudinal diffusivity (e.g., a leak in the hose) are suggestive of neuronal injury or demyelination regardless of mechanism [170]. In radiotherapy, changes in anisotropic diffusion have been noted after radical treatment for gliomas and also retrospectively in pediatric patients who underwent whole brain radiotherapy. These changes have been correlated with decline in neurocognitive tests, compared to pretreatment or healthy controls, suggesting permanent neuronal damage [171, 172]. The ability to distinguish individual nerve tracts and identify those compromised by tumor suggests a method of improved tumor delineation and also a means of identifying eloquent, intact neuronal pathways. A planning study in 13 glioblastoma multiforme patients by Berberat et al. showed a mean reduction in CTV volume of 50 % ($p < 0.005$) was achieved using DTI-based delineations as compared to T2-weighted imaging alone [173]. Prospective implementation of neuronal pathway imaging has been utilized in radiosurgical series, demonstrating low rates of neurologic complication in the treatment of arterial-venous malformations and an improvement of motor dysfunction as compared to the absence of DTI imaging [174, 175]. The integration of DTI into areas outside the brain is lacking, but the rise in spinal stereotactic treatments offers an intriguing potential application.

Summary

Improving the healthy tissue repair profile is critical to minimizing radiation toxicity and thereby widening the therapeutic ratio. The surest way of implementing this goal is to decrease the radiotherapy delivered to normal tissue and particularly highly functional subunits of healthy tissue. The implementation of MRS, hMRS, and DTI has shown promise of not only providing functional information and assisting accurate delineation of tumor invasion but also for directly imaging the function of surrounding anatomy. This has been most developed in the area of brain imaging via neuronal mapping (DTI) and lung through ventilation/perfusion mapping via hMRS. Future work will entail prospective patient data to support improvement of the therapeutic ratio and extension into other body sites.

Technical Considerations

The integration of functional imaging technology into the radiotherapy workflow offers not only additional information to guide treatment planning but also the potential of a new paradigm in radiation oncology practice. However, there exist a number of technical and practical limitations in each of these new imaging modalities; these will require a thorough understanding and characterization prior to full realization of this goal. Many of these limitations apply to all of the techniques described in this chapter and will be reviewed together here.

Simulation

The current radiotherapy workflow as discussed at the beginning of this chapter is based on CT simulation, whereby the patient is positioned on a flat table top and immobilized in the treatment position. This allows for the planning image to represent the daily treatment reality, offering a reproducible environment to derive safety margins. CT simulation is generally fast, on the order of seconds or minutes for four-dimensional acquisitions. Functional imaging modalities described in this chapter often require additional hardware (PET/MRI) that may or may not accommodate treatment immobilization and/or positioning. Both PET and functional MRI often require lengthy scan times depending on the intended image set(s), typically between 20 and 60 min [23, 95]. During this time patients can move, shift, or cough, resulting in degraded image accuracy. These sources of uncertainty must be accounted for in radiotherapy planning to ensure appropriate tumor coverage, particularly when curative doses are intended. Commonly, these uncertainties are incorporated via additional safety margins within the PTV. This results in larger treatment volumes, more irradiated healthy tissue, and therefore increased toxicity, opposite the therapeutic goals. Developments are being made in these areas, with radiotherapy centers increasingly acquiring dedicated imaging equipment (modified to accommodate patient positioning/immobilization) and optimizing image acquisition techniques to reduce scan times [176–178].

Resolution and Registration

Current anatomical CT and MRI scans allow for high-resolution acquisitions, up to 1–2 mm^3 when required, to enable high-precision anatomical delineation and radiation planning. Many of the functional imaging modalities can only acquire images with much coarser pixilation to maintain an adequate signal-to-noise ratio. Not only does this make it difficult to register images, the volume averaging effect can also blur functional features at a tumor's edge. This can be even more pronounced at

tissue interfaces. How one interprets a high-resolution anatomic scan together with a lower resolution but perhaps more biologically relevant image remains uncertain. In addition to spatial resolution, the issue of temporal resolution also exists. There is much literature to suggest that metabolism, proliferation, hypoxia, and repair are not static processes and can change significantly during the course of treatment [119, 179, 180]. When is the right time to image and is a single baseline scan all that is required, or should plans be adapted during treatment? If a biologic feature is targeted, over what time frame is that volume relevant? These are questions that will require further study to adequately address. Relevant reviews addressing these issues for glycolytic and hypoxia-based PET modalities as they relate to the radiotherapy workflow are provided by Scripes and Thorwarth [181, 182]. These issues are further accentuated when merging or fusing multiple imaging modalities together into a single viewable series; where in addition to resolution, deformation becomes prevalent. This can happen between scans on different modalities and also within a single modality throughout time. Whether the tissue is expanding, shrinking, or simply changing shape, the effect on target volumes, both anatomic and biologic, and how they relate to a planned dose distribution will be critical for integrative and adaptive radiotherapy. There is much work focusing on deformable registration algorithms both for intra- and inter-imaging modality, but wide clinical implementation and verification is still incomplete [183–185].

A related issue to resolution is spatial/geometric distortion. While generally not an issue for CT- or PET-based imaging modalities, this can be a large problem in MRI. Distortions in MRI are generally related to inhomogeneities in the main magnetic field and nonlinearities in localizing gradient pulses. These distortions can be intrinsic to scanner-specific field generation, in which case they can usually be modeled and overcome, or by insertion of a nonuniform object into the magnetic field—which is unavoidable as the goal is to have patients within the scanner. As these artifacts are unique to each shape, they can be more difficult to systematically address. In diagnostic radiology, these distortions may not represent a significant issue, as description and identification of disease may depend less on robust spatial integrity; however in targeted radiotherapy, precision and accuracy are of the utmost importance. There are ongoing efforts to develop more robust MRI sequences specifically to address this problem, as well as MRI phantoms to verify spatial accuracy [186, 187]; however, the default radiotherapy reaction is as before to increase safety margins, which again is ultimately counterproductive.

Verification

A key aspect in reducing uncertainties (and therefore volumes) in radiotherapy is the treatment verification process, where daily setup is compared to and adjusted according to treatment planning scans. The precision of this task is directly related to the PTV margin utilized in patient planning. Currently the radiotherapy workflow is organized around CT-based planning and daily verification via orthogonal

X-rays, megavoltage portal films, or volumetric cone-beam CT scans. This practice is relatively robust as image comparison among X-ray-based modalities is straightforward. Introduction of functional imaging modalities, particularly MRI based, represents a new challenge for daily verification. The most utilized approach is to verify registration between planning scan and the adjunct planning images, leaving daily verification solely X-ray based. As discussed above, this approach has several shortcomings and the alternative is again to increase the PTV margin. Ongoing work toward MRI-based verification scans in MRI-linac systems offers perhaps a better solution to this problem [188–190].

Summary

Functional imaging and the capability to target and optimize treatment plans according to biology in addition to anatomy represent an exciting new area in radiation oncology. However, a number of technical challenges must be considered before true integration can take place. Questions remain on when the optimal time is to obtain biologic imaging (and whether this needs to be repeated during treatment), how to incorporate radiotherapy immobilization, how precise image registration is (± deformation), and how to verify daily treatment position. With ongoing development of new imaging modalities and new radiotherapy delivery platforms, these questions will hopefully be addressed.

Conclusion

Since its inception, radiation oncology has been an image-guided treatment modality. Advances in imaging technology have allowed for the direct visualization and quantification of biologic processes critical to therapy response. This chapter has outlined and summarized a variety of these techniques including PET (with a variety of tracers), diffusion- and contrast-based MRI (and CT), and spectroscopy, organized by three of the classic tenants of radiobiology: *r*epopulation, *r*eoxygenation, and *r*epair. The ability to better delineate and target tumors according to their biologic underpinnings and specifically how they enhance or compromise interactions with radiotherapy will allow further personalization of patient care. Retrospective and ongoing prospective studies investigating these interactions have shown promising results in terms of tumor control and treatment toxicity. The long-term viability of this strategy will depend on the maturation of these and future studies, as well as overcoming current technical limitations, including spatial-temporal resolution and workflow integration. With ongoing effort, the goal of multimodality-based radiotherapy is achievable and can potentially provide a fulcrum to further tilt the therapeutic ratio in the patients' favor.

References

1. Nakamura K et al (2014) Recent advances in radiation oncology: intensity-modulated radiotherapy, a clinical perspective. Int J Clin Oncol 19(4):564–569
2. Hodapp N (2012) The ICRU Report 83: prescribing, recording and reporting photon-beam intensity-modulated radiation therapy (IMRT). Strahlenther Onkol 188(1):97–99
3. Ling CC, Li XA (2005) Over the next decade the success of radiation treatment planning will be judged by the immediate biological response of tumor cells rather than by surrogate measures such as dose maximization and uniformity. Med Phys 32(7):2189–2192
4. Bentzen SM (2005) Theragnostic imaging for radiation oncology: dose-painting by numbers. Lancet Oncol 6(2):112–117
5. Withers HR (1985) Biologic basis for altered fractionation schemes. Cancer 55(Suppl 9): 2086–2095
6. Steel GG (1996) From targets to genes: a brief history of radiosensitivity. Phys Med Biol 41(2):205–222
7. Harrington K, Jankowska P, Hingorani M (2007) Molecular biology for the radiation oncologist: the 5Rs of radiobiology meet the hallmarks of cancer. Clin Oncol (R Coll Radiol) 19(8): 561–571
8. Hanahan D, Weinberg RA (2000) The hallmarks of cancer. Cell 100(1):57–70
9. Fischer BM, Lassen U, Hojgaard L (2011) PET-CT in preoperative staging of lung cancer. N Engl J Med 364(10):980–981
10. Schmidt T et al (2015) Value of functional imaging by PET in esophageal cancer. J Natl Compr Canc Netw 13(2):239–247
11. Ng SH et al (2008) Distant metastases and synchronous second primary tumors in patients with newly diagnosed oropharyngeal and hypopharyngeal carcinomas: evaluation of (18) F-FDG PET and extended-field multi-detector row CT. Neuroradiology 50(11):969–979
12. Abramyuk A et al (2013) Modification of staging and treatment of head and neck cancer by FDG-PET/CT prior to radiotherapy. Strahlenther Onkol 189(3):197–201
13. Gallamini A, Borra A (2014) Role of PET in lymphoma. Curr Treat Options Oncol 15(2): 248–261
14. Calais J et al (2015) Areas of high 18F-FDG uptake on preradiotherapy PET/CT identify preferential sites of local relapse after chemoradiotherapy for non-small cell lung cancer. J Nucl Med 56(2):196–203
15. Bradley J et al (2004) Impact of FDG-PET on radiation therapy volume delineation in non-small-cell lung cancer. Int J Radiat Oncol Biol Phys 59(1):78–86
16. Roh JL et al (2014) Clinical significance of pretreatment metabolic tumor volume and total lesion glycolysis in hypopharyngeal squamous cell carcinomas. J Surg Oncol 110(7): 869–875
17. Due AK et al (2014) Recurrences after intensity modulated radiotherapy for head and neck squamous cell carcinoma more likely to originate from regions with high baseline [18F]-FDG uptake. Radiother Oncol 111(3):360–365
18. Hoeben BA et al (2013) Molecular PET imaging for biology-guided adaptive radiotherapy of head and neck cancer. Acta Oncol 52(7):1257–1271
19. van Stiphout RG et al (2014) Nomogram predicting response after chemoradiotherapy in rectal cancer using sequential PETCT imaging: a multicentric prospective study with external validation. Radiother Oncol 113(2):215–222
20. Schollaert P et al (2014) A systematic review of the predictive value of (18)FDG-PET in esophageal and esophagogastric junction cancer after neoadjuvant chemoradiation on the survival outcome stratification. J Gastrointest Surg 18(5):894–905
21. Engert A et al (2012) Reduced-intensity chemotherapy and PET-guided radiotherapy in patients with advanced stage Hodgkin's lymphoma (HD15 trial): a randomised, open-label, phase 3 non-inferiority trial. Lancet 379(9828):1791–1799

22. Raemaekers JM et al (2014) Omitting radiotherapy in early positron emission tomography-negative stage I/II Hodgkin lymphoma is associated with an increased risk of early relapse: clinical results of the preplanned interim analysis of the randomized EORTC/LYSA/FIL H10 trial. J Clin Oncol 32(12):1188–1194
23. Jelercic S, Rajer M (2015) The role of PET-CT in radiotherapy planning of solid tumours. Radiol Oncol 49(1):1–9
24. Kilic D et al (2015) Is there any impact of PET/CT on radiotherapy planning in rectal cancer patients undergoing preoperative IMRT? Turk J Med Sci 45(1):129–135
25. Vojtisek R et al (2014) The impact of PET/CT scanning on the size of target volumes, radiation exposure of organs at risk, TCP and NTCP, in the radiotherapy planning of non-small cell lung cancer. Rep Pract Oncol Radiother 19(3):182–190
26. Nkhali L et al (2015) FDG-PET/CT during concomitant chemo radiotherapy for esophageal cancer: reducing target volumes to deliver higher radiotherapy doses. Acta Oncol 54(6): 909–915
27. Daisne JF et al (2004) Tumor volume in pharyngolaryngeal squamous cell carcinoma: comparison at CT, MR imaging, and FDG PET and validation with surgical specimen. Radiology 233(1):93–100
28. Madani I et al (2011) Maximum tolerated dose in a phase I trial on adaptive dose painting by numbers for head and neck cancer. Radiother Oncol 101(3):351–355
29. Yu W et al (2015) Safety of dose escalation by simultaneous integrated boosting radiation dose within the primary tumor guided by (18)FDG-PET/CT for esophageal cancer. Radiother Oncol 114(2):195–200
30. van Der Wel A et al (2005) Increased therapeutic ratio by 18FDG-PET CT planning in patients with clinical CT stage N2-N3M0 non-small-cell lung cancer: a modeling study. Int J Radiat Oncol Biol Phys 61(3):649–655
31. van Elmpt W et al (2012) The PET-boost randomised phase II dose-escalation trial in non-small cell lung cancer. Radiother Oncol 104(1):67–71
32. Shi X et al (2014) PET/CT imaging-guided dose painting in radiation therapy. Cancer Lett 355(2):169–175
33. Mukundan H et al (2014) MRI and PET-CT: comparison in post-treatment evaluation of head and neck squamous cell carcinomas. Med J Armed Forces India 70(2):111–115
34. Kauppi JT et al (2012) Locally advanced esophageal adenocarcinoma: response to neoadjuvant chemotherapy and survival predicted by ([18F])FDG-PET/CT. Acta Oncol 51(5):636–644
35. Bahce I et al (2014) Metabolic activity measured by FDG PET predicts pathological response in locally advanced superior sulcus NSCLC. Lung Cancer 85(2):205–212
36. Schwarz JK et al (2012) Metabolic response on post-therapy FDG-PET predicts patterns of failure after radiotherapy for cervical cancer. Int J Radiat Oncol Biol Phys 83(1):185–190
37. Pathmanathan N, Balleine RL (2013) Ki67 and proliferation in breast cancer. J Clin Pathol 66(6):512–516
38. Wang XW, Zhang YJ (2014) Targeting mTOR network in colorectal cancer therapy. World J Gastroenterol 20(15):4178–4188
39. Ruschoff J et al (1996) Prognostic significance of molecular biological and immunohistological parameters in gastrointestinal carcinomas. Recent Results Cancer Res 142:73–88
40. Skalova A, Leivo I (1996) Cell proliferation in salivary gland tumors. Gen Diagn Pathol 142(1):7–16
41. Kim JJ, Tannock IF (2005) Repopulation of cancer cells during therapy: an important cause of treatment failure. Nat Rev Cancer 5(7):516–525
42. Janssen S et al (2009) Anal cancer treated with radio-chemotherapy: correlation between length of treatment interruption and outcome. Int J Colorectal Dis 24(12):1421–1428
43. Duncan W et al (1996) Adverse effect of treatment gaps in the outcome of radiotherapy for laryngeal cancer. Radiother Oncol 41(3):203–207

44. Moonen L et al (1998) Muscle-invasive bladder cancer treated with external beam radiation: influence of total dose, overall treatment time, and treatment interruption on local control. Int J Radiat Oncol Biol Phys 42(3):525–530
45. Fyles A et al (1992) The effect of treatment duration in the local control of cervix cancer. Radiother Oncol 25(4):273–279
46. Robertson C et al (1998) Similar decreases in local tumor control are calculated for treatment protraction and for interruptions in the radiotherapy of carcinoma of the larynx in four centers. Int J Radiat Oncol Biol Phys 40(2):319–329
47. Nakajo M et al (2014) Correlations of (18)F-fluorothymidine uptake with pathological tumour size, Ki-67 and thymidine kinase 1 expressions in primary and metastatic lymph node colorectal cancer foci. Eur Radiol 24(12):3199–3209
48. Yamamoto Y et al (2012) Correlation of 18F-FLT uptake with tumor grade and Ki-67 immunohistochemistry in patients with newly diagnosed and recurrent gliomas. J Nucl Med 53(12):1911–1915
49. Woolf DK et al (2014) Evaluation of FLT-PET-CT as an imaging biomarker of proliferation in primary breast cancer. Br J Cancer 110(12):2847–2854
50. Hoeben BA et al (2013) 18F-FLT PET during radiotherapy or chemoradiotherapy in head and neck squamous cell carcinoma is an early predictor of outcome. J Nucl Med 54(4):532–540
51. Zander T et al (2011) Early prediction of nonprogression in advanced non-small-cell lung cancer treated with erlotinib by using [(18)F]fluorodeoxyglucose and [(18)F]fluorothymidine positron emission tomography. J Clin Oncol 29(13):1701–1708
52. Everitt SJ et al (2014) Differential 18F-FDG and 18F-FLT uptake on serial PET/CT imaging before and during definitive chemoradiation for non-small cell lung cancer. J Nucl Med 55(7):1069–1074
53. Zhang G et al (2015) Gradient-based delineation of the primary GTV on FLT PET in squamous cell cancer of the thoracic esophagus and impact on radiotherapy planning. Radiat Oncol 10(1):11
54. Patel DA et al (2007) Impact of integrated PET/CT on variability of target volume delineation in rectal cancer. Technol Cancer Res Treat 6(1):31–36
55. Troost EG et al (2010) 18F-FLT PET/CT for early response monitoring and dose escalation in oropharyngeal tumors. J Nucl Med 51(6):866–874
56. Tehrani OS, Shields AF (2013) PET imaging of proliferation with pyrimidines. J Nucl Med 54(6):903–912
57. Contractor K et al (2011) Use of [11C]choline PET-CT as a noninvasive method for detecting pelvic lymph node status from prostate cancer and relationship with choline kinase expression. Clin Cancer Res 17(24):7673–7683
58. Chan J et al (2015) Is choline PET useful for identifying intraprostatic tumour lesions? A literature review. Nucl Med Commun
59. Chang JH et al (2012) Intensity modulated radiation therapy dose painting for localized prostate cancer using (1)(1)C-choline positron emission tomography scans. Int J Radiat Oncol Biol Phys 83(5):e691–e696
60. Niyazi M et al (2010) Choline PET based dose-painting in prostate cancer—modelling of dose effects. Radiat Oncol 5:23
61. Pinkawa M et al (2012) Dose-escalation using intensity-modulated radiotherapy for prostate cancer—evaluation of quality of life with and without (18)F-choline PET-CT detected simultaneous integrated boost. Radiat Oncol 7:14
62. Goldstein J et al (2014) Does choline PET/CT change the management of prostate cancer patients with biochemical failure? Am J Clin Oncol
63. Alongi F et al (2014) 11C choline PET guided salvage radiotherapy with volumetric modulation arc therapy and hypofractionation for recurrent prostate cancer after HIFU failure: preliminary results of tolerability and acute toxicity. Technol Cancer Res Treat 13(5):395–401
64. Hamstra DA, Rehemtulla A, Ross BD (2007) Diffusion magnetic resonance imaging: a biomarker for treatment response in oncology. J Clin Oncol 25(26):4104–4109

65. Thoeny HC, De Keyzer F, King AD (2012) Diffusion-weighted MR imaging in the head and neck. Radiology 263(1):19–32
66. Thoeny HC, Forstner R, De Keyzer F (2012) Genitourinary applications of diffusion-weighted MR imaging in the pelvis. Radiology 263(2):326–342
67. Petralia G, Thoeny HC (2010) DW-MRI of the urogenital tract: applications in oncology. Cancer Imaging 10(Spec no A):S112–S123
68. Mascalchi M et al (2005) Diffusion-weighted MR of the brain: methodology and clinical application. Radiol Med 109(3):155–197
69. Sevcenco S et al (2014) Quantitative apparent diffusion coefficient measurements obtained by 3-Tesla MRI are correlated with biomarkers of bladder cancer proliferative activity. PLoS One 9(9), e106866
70. Cipolla V et al (2014) Correlation between 3T apparent diffusion coefficient values and grading of invasive breast carcinoma. Eur J Radiol 83(12):2144–2150
71. Kim EJ et al (2015) Histogram analysis of apparent diffusion coefficient at 3.0t: correlation with prognostic factors and subtypes of invasive ductal carcinoma. J Magn Reson Imaging
72. Donati OF et al (2014) Prostate cancer aggressiveness: assessment with whole-lesion histogram analysis of the apparent diffusion coefficient. Radiology 271(1):143–152
73. Woo S et al (2014) Histogram analysis of apparent diffusion coefficient map of diffusion-weighted MRI in endometrial cancer: a preliminary correlation study with histological grade. Acta Radiol 55(10):1270–1277
74. Rothke M et al (2013) PI-RADS classification: structured reporting for MRI of the prostate. Röfo 185(3):253–261
75. Futterer JJ et al (2015) Can clinically significant prostate cancer be detected with multiparametric magnetic resonance imaging? A systematic review of the literature. Eur Urol 68(6): 1045–1053
76. Micco M et al (2014) Combined pre-treatment MRI and 18F-FDG PET/CT parameters as prognostic biomarkers in patients with cervical cancer. Eur J Radiol 83(7):1169–1176
77. Nakamura K et al (2012) The mean apparent diffusion coefficient value (ADCmean) on primary cervical cancer is a predictive marker for disease recurrence. Gynecol Oncol 127(3): 478–483
78. Kuang F et al (2013) The value of apparent diffusion coefficient in the assessment of cervical cancer. Eur Radiol 23(4):1050–1058
79. Chopra S et al (2012) Evaluation of diffusion-weighted imaging as a predictive marker for tumor response in patients undergoing chemoradiation for postoperative recurrences of cervical cancer. J Cancer Res Ther 8(1):68–73
80. Joye I et al (2014) The role of diffusion-weighted MRI and (18)F-FDG PET/CT in the prediction of pathologic complete response after radiochemotherapy for rectal cancer: a systematic review. Radiother Oncol 113(2):158–165
81. Yu JI et al (2014) The role of diffusion-weighted magnetic resonance imaging in the treatment response evaluation of hepatocellular carcinoma patients treated with radiation therapy. Int J Radiat Oncol Biol Phys 89(4):814–821
82. Hamstra DA et al (2008) Functional diffusion map as an early imaging biomarker for high-grade glioma: correlation with conventional radiologic response and overall survival. J Clin Oncol 26(20):3387–3394
83. Galban CJ et al (2009) A feasibility study of parametric response map analysis of diffusion-weighted magnetic resonance imaging scans of head and neck cancer patients for providing early detection of therapeutic efficacy. Transl Oncol 2(3):184–190
84. Chen Y et al (2014) Diffusion-weighted magnetic resonance imaging for early response assessment of chemoradiotherapy in patients with nasopharyngeal carcinoma. Magn Reson Imaging 32(6):630–637
85. Eccles CL et al (2009) Change in diffusion weighted MRI during liver cancer radiotherapy: preliminary observations. Acta Oncol 48(7):1034–1043

86. Sun YS et al (2010) Locally advanced rectal carcinoma treated with preoperative chemotherapy and radiation therapy: preliminary analysis of diffusion-weighted MR imaging for early detection of tumor histopathologic downstaging. Radiology 254(1):170–178
87. Kim SH et al (2011) Apparent diffusion coefficient for evaluating tumour response to neoadjuvant chemoradiation therapy for locally advanced rectal cancer. Eur Radiol 21(5):987–995
88. Cai G et al (2013) Diffusion-weighted magnetic resonance imaging for predicting the response of rectal cancer to neoadjuvant concurrent chemoradiation. World J Gastroenterol 19(33):5520–5527
89. Harry VN et al (2008) Diffusion-weighted magnetic resonance imaging in the early detection of response to chemoradiation in cervical cancer. Gynecol Oncol 111(2):213–220
90. Kim HS et al (2013) Evaluation of therapeutic response to concurrent chemoradiotherapy in patients with cervical cancer using diffusion-weighted MR imaging. J Magn Reson Imaging 37(1):187–193
91. Fu C et al (2012) The value of diffusion-weighted magnetic resonance imaging in assessing the response of locally advanced cervical cancer to neoadjuvant chemotherapy. Int J Gynecol Cancer 22(6):1037–1043
92. Fu ZZ et al (2015) Value of apparent diffusion coefficient (ADC) in assessing radiotherapy and chemotherapy success in cervical cancer. Magn Reson Imaging 33(5):516–524
93. Liney GP et al (2015) Quantitative evaluation of diffusion-weighted imaging techniques for the purposes of radiotherapy planning in the prostate. Br J Radiol 88(1049):20150034
94. Regini F et al (2014) Rectal tumour volume (GTV) delineation using T2-weighted and diffusion-weighted MRI: implications for radiotherapy planning. Eur J Radiol 83(5):768–772
95. Tsien C, Cao Y, Chenevert T (2014) Clinical applications for diffusion magnetic resonance imaging in radiotherapy. Semin Radiat Oncol 24(3):218–226
96. Walsh JC et al (2014) The clinical importance of assessing tumor hypoxia: relationship of tumor hypoxia to prognosis and therapeutic opportunities. Antioxid Redox Signal 21(10):1516–1554
97. Peitzsch C et al (2014) Hypoxia as a biomarker for radioresistant cancer stem cells. Int J Radiat Biol 90(8):636–652
98. Vaupel P, Mayer A (2007) Hypoxia in cancer: significance and impact on clinical outcome. Cancer Metastasis Rev 26(2):225–239
99. Overgaard J (2011) Hypoxic modification of radiotherapy in squamous cell carcinoma of the head and neck—a systematic review and meta-analysis. Radiother Oncol 100(1):22–32
100. Overgaard J (2007) Hypoxic radiosensitization: adored and ignored. J Clin Oncol 25(26): 4066–4074
101. Brizel DM et al (1996) Radiation therapy and hyperthermia improve the oxygenation of human soft tissue sarcomas. Cancer Res 56(23):5347–5350
102. Fyles AW et al (1998) Cervix cancer oxygenation measured following external radiation therapy. Int J Radiat Oncol Biol Phys 42(4):751–753
103. Chapman JD (1979) Hypoxic sensitizers—implications for radiation therapy. N Engl J Med 301(26):1429–1432
104. Mortensen LS et al (2012) FAZA PET/CT hypoxia imaging in patients with squamous cell carcinoma of the head and neck treated with radiotherapy: results from the DAHANCA 24 trial. Radiother Oncol 105(1):14–20
105. Thorwarth D et al (2005) Kinetic analysis of dynamic 18F-fluoromisonidazole PET correlates with radiation treatment outcome in head-and-neck cancer. BMC Cancer 5:152
106. Chang E et al (2014) 18F-FAZA PET imaging response tracks the reoxygenation of tumors in mice upon treatment with the mitochondrial complex I inhibitor BAY 87-2243. Clin Cancer Res 21(2):335–346
107. Zips D et al (2012) Exploratory prospective trial of hypoxia-specific PET imaging during radiochemotherapy in patients with locally advanced head-and-neck cancer. Radiother Oncol 105(1):21–28
108. Dehdashti F et al (2008) Assessing tumor hypoxia in cervical cancer by PET with 60Cu-labeled diacetyl-bis(N4-methylthiosemicarbazone). J Nucl Med 49(2):201–205

109. Kikuchi M et al (2011) 18F-fluoromisonidazole positron emission tomography before treatment is a predictor of radiotherapy outcome and survival prognosis in patients with head and neck squamous cell carcinoma. Ann Nucl Med 25(9):625–633
110. Vercellino L et al (2012) Hypoxia imaging of uterine cervix carcinoma with (18)F-FETNIM PET/CT. Clin Nucl Med 37(11):1065–1068
111. Li L et al (2010) Comparison of 18F-Fluoroerythronitroimidazole and 18F-fluorodeoxyglucose positron emission tomography and prognostic value in locally advanced non-small-cell lung cancer. Clin Lung Cancer 11(5):335–340
112. Rajendran JG et al (2006) Tumor hypoxia imaging with [F-18] fluoromisonidazole positron emission tomography in head and neck cancer. Clin Cancer Res 12(18):5435–5441
113. Spence AM et al (2008) Regional hypoxia in glioblastoma multiforme quantified with [18F] fluoromisonidazole positron emission tomography before radiotherapy: correlation with time to progression and survival. Clin Cancer Res 14(9):2623–2630
114. Horsman MR et al (2012) Imaging hypoxia to improve radiotherapy outcome. Nat Rev Clin Oncol 9(12):674–687
115. Servagi-Vernat S et al (2015) Hypoxia-guided adaptive radiation dose escalation in head and neck carcinoma: a planning study. Acta Oncol 54(7):1008–1016
116. Chang JH et al (2013) Hypoxia-targeted radiotherapy dose painting for head and neck cancer using (18)F-FMISO PET: a biological modeling study. Acta Oncol 52(8):1723–1729
117. Henriques de Figueiredo B et al (2015) Hypoxia imaging with [18F]-FMISO-PET for guided dose escalation with intensity-modulated radiotherapy in head-and-neck cancers. Strahlenther Onkol 191(3):217–224
118. Lin Z et al (2008) The influence of changes in tumor hypoxia on dose-painting treatment plans based on 18F-FMISO positron emission tomography. Int J Radiat Oncol Biol Phys 70(4):1219–1228
119. Bollineni VR et al (2014) Dynamics of tumor hypoxia assessed by 18F-FAZA PET/CT in head and neck and lung cancer patients during chemoradiation: possible implications for radiotherapy treatment planning strategies. Radiother Oncol 113(2):198–203
120. Helbig L et al (2014) BAY 87-2243, a novel inhibitor of hypoxia-induced gene activation, improves local tumor control after fractionated irradiation in a schedule-dependent manner in head and neck human xenografts. Radiat Oncol 9:207
121. Beck R et al (2007) Pretreatment 18F-FAZA PET predicts success of hypoxia-directed radiochemotherapy using tirapazamine. J Nucl Med 48(6):973–980
122. Padhani A (2006) PET imaging of tumour hypoxia. Cancer Imaging 6:S117–S121
123. Fleming IN et al (2015) Imaging tumour hypoxia with positron emission tomography. Br J Cancer 112(2):238–250
124. Cooper RA et al (2000) Tumour oxygenation levels correlate with dynamic contrast-enhanced magnetic resonance imaging parameters in carcinoma of the cervix. Radiother Oncol 57(1): 53–59
125. Mayr NA et al (1996) Tumor perfusion studies using fast magnetic resonance imaging technique in advanced cervical cancer: a new noninvasive predictive assay. Int J Radiat Oncol Biol Phys 36(3):623–633
126. Borren A et al (2013) Expression of hypoxia-inducible factor-1alpha and -2alpha in whole-mount prostate histology: relation with dynamic contrast-enhanced MRI and Gleason score. Oncol Rep 29(6):2249–2254
127. Ellingsen C et al (2014) DCE-MRI of the hypoxic fraction, radioresponsiveness, and metastatic propensity of cervical carcinoma xenografts. Radiother Oncol 110(2):335–341
128. Linnik IV et al (2014) Noninvasive tumor hypoxia measurement using magnetic resonance imaging in murine U87 glioma xenografts and in patients with glioblastoma. Magn Reson Med 71(5):1854–1862
129. Halle C et al (2012) Hypoxia-induced gene expression in chemoradioresistant cervical cancer revealed by dynamic contrast-enhanced MRI. Cancer Res 72(20):5285–5295

130. Mayr NA et al (2000) Pixel analysis of MR perfusion imaging in predicting radiation therapy outcome in cervical cancer. J Magn Reson Imaging 12(6):1027–1033
131. Mayr NA et al (2010) Longitudinal changes in tumor perfusion pattern during the radiation therapy course and its clinical impact in cervical cancer. Int J Radiat Oncol Biol Phys 77(2):502–508
132. van Lin EN et al (2006) IMRT boost dose planning on dominant intraprostatic lesions: gold marker-based three-dimensional fusion of CT with dynamic contrast-enhanced and 1H-spectroscopic MRI. Int J Radiat Oncol Biol Phys 65(1):291–303
133. Garibaldi E et al (2016) Clinical and technical feasibility of ultra-boost irradiation in Dominant Intraprostatic Lesion by Tomotherapy: preliminary experience and revision of literature. Panminerva Med 58(1):16–22
134. Lips IM et al (2011) Single blind randomized phase III trial to investigate the benefit of a focal lesion ablative microboost in prostate cancer (FLAME-trial): study protocol for a randomized controlled trial. Trials 12:255
135. Hallac RR et al (2014) Correlations of noninvasive BOLD and TOLD MRI with pO2 and relevance to tumor radiation response. Magn Reson Med 71(5):1863–1873
136. Al-Hallaq HA et al (2000) MRI measurements correctly predict the relative effects of tumor oxygenating agents on hypoxic fraction in rodent BA1112 tumors. Int J Radiat Oncol Biol Phys 47(2):481–488
137. Toth V et al (2013) MR-based hypoxia measures in human glioma. J Neurooncol 115(2): 197–207
138. Liu M et al (2013) BOLD-MRI of breast invasive ductal carcinoma: correlation of R2* value and the expression of HIF-1alpha. Eur Radiol 23(12):3221–3227
139. Chopra S et al (2009) Comparing oxygen-sensitive MRI (BOLD R2*) with oxygen electrode measurements: a pilot study in men with prostate cancer. Int J Radiat Biol 85(9):805–813
140. Sovik A et al (2007) Radiotherapy adapted to spatial and temporal variability in tumor hypoxia. Int J Radiat Oncol Biol Phys 68(5):1496–1504
141. Matsuo M et al (2014) Magnetic resonance imaging of the tumor microenvironment in radiotherapy: perfusion, hypoxia, and metabolism. Semin Radiat Oncol 24(3):210–217
142. Mandeville HC et al (2012) Operable non-small cell lung cancer: correlation of volumetric helical dynamic contrast-enhanced CT parameters with immunohistochemical markers of tumor hypoxia. Radiology 264(2):581–589
143. Newbold K et al (2009) An exploratory study into the role of dynamic contrast-enhanced magnetic resonance imaging or perfusion computed tomography for detection of intratumoral hypoxia in head-and-neck cancer. Int J Radiat Oncol Biol Phys 74(1):29–37
144. Nyflot MJ et al (2015) Phase 1 trial of bevacizumab with concurrent chemoradiation therapy for squamous cell carcinoma of the head and neck with exploratory functional imaging of tumor hypoxia, proliferation, and perfusion. Int J Radiat Oncol Biol Phys 91(5):942–951
145. Yeung TP et al (2015) Survival prediction in high-grade gliomas using CT perfusion imaging. J Neurooncol 123(1):93–102
146. van Elmpt W et al (2014) Imaging techniques for tumour delineation and heterogeneity quantification of lung cancer: overview of current possibilities. J Thorac Dis 6(4):319–327
147. Astner ST et al (2010) Imaging of tumor physiology: impacts on clinical radiation oncology. Exp Oncol 32(3):149–152
148. Shibata A, Jeggo PA (2014) DNA double-strand break repair in a cellular context. Clin Oncol (R Coll Radiol) 26(5):243–249
149. Tamulevicius P, Wang M, Iliakis G (2007) Homology-directed repair is required for the development of radioresistance during S phase: interplay between double-strand break repair and checkpoint response. Radiat Res 167(1):1–11
150. Crawford FW et al (2009) Relationship of pre-surgery metabolic and physiological MR imaging parameters to survival for patients with untreated GBM. J Neurooncol 91(3):337–351
151. Saraswathy S et al (2009) Evaluation of MR markers that predict survival in patients with newly diagnosed GBM prior to adjuvant therapy. J Neurooncol 91(1):69–81

152. Ken S et al (2013) Integration method of 3D MR spectroscopy into treatment planning system for glioblastoma IMRT dose painting with integrated simultaneous boost. Radiat Oncol 8:1
153. Einstein DB et al (2012) Phase II trial of radiosurgery to magnetic resonance spectroscopy-defined high-risk tumor volumes in patients with glioblastoma multiforme. Int J Radiat Oncol Biol Phys 84(3):668–674
154. Jahangiri A, Aghi MK (2012) Pseudoprogression and treatment effect. Neurosurg Clin N Am 23(2):277–287, viii–ix
155. Huang J et al (2011) Differentiation between intra-axial metastatic tumor progression and radiation injury following fractionated radiation therapy or stereotactic radiosurgery using MR spectroscopy, perfusion MR imaging or volume progression modeling. Magn Reson Imaging 29(7):993–1001
156. Elias AE et al (2011) MR spectroscopy using normalized and non-normalized metabolite ratios for differentiating recurrent brain tumor from radiation injury. Acad Radiol 18(9):1101–1108
157. Zhang H et al (2014) Role of magnetic resonance spectroscopy for the differentiation of recurrent glioma from radiation necrosis: a systematic review and meta-analysis. Eur J Radiol 83(12):2181–2189
158. Mueller-Lisse UG, Scherr MK (2007) Proton MR spectroscopy of the prostate. Eur J Radiol 63(3):351–360
159. Yuen JS et al (2004) Endorectal magnetic resonance imaging and spectroscopy for the detection of tumor foci in men with prior negative transrectal ultrasound prostate biopsy. J Urol 171(4):1482–1486
160. Selnaes KM et al (2013) Spatially matched in vivo and ex vivo MR metabolic profiles of prostate cancer—investigation of a correlation with Gleason score. NMR Biomed 26(5): 600–606
161. DiBiase SJ et al (2002) Magnetic resonance spectroscopic imaging-guided brachytherapy for localized prostate cancer. Int J Radiat Oncol Biol Phys 52(2):429–438
162. Pickett B et al (1999) Static field intensity modulation to treat a dominant intra-prostatic lesion to 90 Gy compared to seven field 3-dimensional radiotherapy. Int J Radiat Oncol Biol Phys 44(4):921–929
163. Riches SF et al (2014) Effect on therapeutic ratio of planning a boosted radiotherapy dose to the dominant intraprostatic tumour lesion within the prostate based on multifunctional MR parameters. Br J Radiol 87(1037):20130813
164. Thind K et al (2014) Mapping metabolic changes associated with early Radiation Induced Lung Injury post conformal radiotherapy using hyperpolarized (1)(3)C-pyruvate Magnetic Resonance Spectroscopic Imaging. Radiother Oncol 110(2):317–322
165. Kauczor HU et al (1996) Normal and abnormal pulmonary ventilation: visualization at hyperpolarized He-3 MR imaging. Radiology 201(2):564–568
166. Hodge CW et al (2010) On the use of hyperpolarized helium MRI for conformal avoidance lung radiotherapy. Med Dosim 35(4):297–303
167. Hoover DA et al (2014) Functional lung avoidance for individualized radiotherapy (FLAIR): study protocol for a randomized, double-blind clinical trial. BMC Cancer 14:934
168. Nguyen ML et al (2014) The potential role of magnetic resonance spectroscopy in image-guided radiotherapy. Front Oncol 4:91
169. Le Bihan D et al (2001) Diffusion tensor imaging: concepts and applications. J Magn Reson Imaging 13(4):534–546
170. Stebbins GT, Murphy CM (2009) Diffusion tensor imaging in Alzheimer's disease and mild cognitive impairment. Behav Neurol 21(1):39–49
171. Chapman CH et al (2012) Diffusion tensor imaging of normal-appearing white matter as biomarker for radiation-induced late delayed cognitive decline. Int J Radiat Oncol Biol Phys 82(5):2033–2040
172. Edelmann MN et al (2014) Diffusion tensor imaging and neurocognition in survivors of childhood acute lymphoblastic leukaemia. Brain 137(Pt 11):2973–2983

173. Berberat J et al (2014) Diffusion tensor imaging for target volume definition in glioblastoma multiforme. Strahlenther Onkol 190(10):939–943
174. Koga T et al (2012) Outcomes of diffusion tensor tractography-integrated stereotactic radiosurgery. Int J Radiat Oncol Biol Phys 82(2):799–802
175. Koga T et al (2012) Integration of corticospinal tractography reduces motor complications after radiosurgery. Int J Radiat Oncol Biol Phys 83(1):129–133
176. Hanvey S, Glegg M, Foster J (2009) Magnetic resonance imaging for radiotherapy planning of brain cancer patients using immobilization and surface coils. Phys Med Biol 54(18):5381–5394
177. Ahmed M et al (2010) The value of magnetic resonance imaging in target volume delineation of base of tongue tumours—a study using flexible surface coils. Radiother Oncol 94(2):161–167
178. Houweling AC et al (2010) Magnetic resonance imaging at 3.0T for submandibular gland sparing radiotherapy. Radiother Oncol 97(2):239–243
179. Houweling AC et al (2013) FDG-PET and diffusion-weighted MRI in head-and-neck cancer patients: implications for dose painting. Radiother Oncol 106(2):250–254
180. Decker G et al (2014) Intensity-modulated radiotherapy of the prostate: dynamic ADC monitoring by DWI at 3.0 T. Radiother Oncol 113(1):115–120
181. Scripes PG, Yaparpalvi R (2012) Technical aspects of positron emission tomography/computed tomography in radiotherapy treatment planning. Semin Nucl Med 42(5):283–288
182. Thorwarth D, Alber M (2010) Implementation of hypoxia imaging into treatment planning and delivery. Radiother Oncol 97(2):172–175
183. Yu G et al (2015) Accelerated gradient-based free form deformable registration for online adaptive radiotherapy. Phys Med Biol 60(7):2765–2783
184. Leibfarth S et al (2013) A strategy for multimodal deformable image registration to integrate PET/MR into radiotherapy treatment planning. Acta Oncol 52(7):1353–1359
185. Niu CJ et al (2012) A novel technique to enable experimental validation of deformable dose accumulation. Med Phys 39(2):765–776
186. Torfeh T et al (2015) Development and validation of a novel large field of view phantom and a software module for the quality assurance of geometric distortion in magnetic resonance imaging. Magn Reson Imaging 33(7):939–949
187. Haack S et al (2014) Correction of diffusion-weighted magnetic resonance imaging for brachytherapy of locally advanced cervical cancer. Acta Oncol 53(8):1073–1078
188. Keall PJ, Barton M, Crozier S (2014) The Australian magnetic resonance imaging-linac program. Semin Radiat Oncol 24(3):203–206
189. Lagendijk JJ, Raaymakers BW, van Vulpen M (2014) The magnetic resonance imaging-linac system. Semin Radiat Oncol 24(3):207–209
190. Jaffray DA et al (2014) A facility for magnetic resonance-guided radiation therapy. Semin Radiat Oncol 24(3):193–195